AFCRL-TR-75-0324

SAI-74-624-WA

POEM: A FAST MONTE CARLO CODE FOR THE CALCULATION OF X-RAY PHOTOEMISSION AND TRANSITION ZONE DOSE AND CURRENT

William L. Chadsey
Science Applications, Incorporated
1651 Old Meadow Road
McLean, Virginia 22101

15 January 1975

Scientific Report No. 1

This research was sponsored by the Defense Nuclear Agency under Subtask Z99QAXTA040, Work Unit 51, entitled "Secondary Electron Transport Phenomenology."

AIR FORCE CAMBRIDGE RESEARCH LABORATORIES
AIR FORCE SYSTEMS COMMAND
UNITED STATES AIR FORCE
HANSCOM AFB, MASSACHUSETTS 01731

Qualified requestors may obtain additional copies from the Defense Documentation Center.

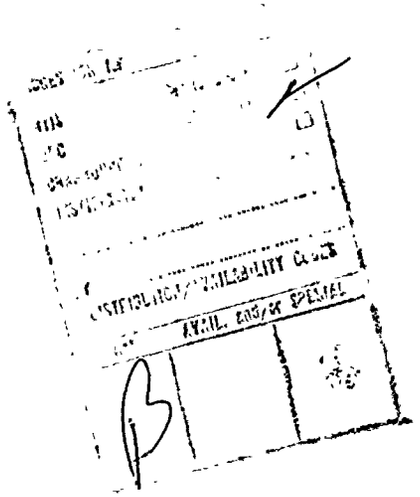

UNCLASSIFIED

SECURITY CLASSIFICATION OF THIS PAGE *(When Data Entered)*

REPORT DOCUMENTATION PAGE	READ INSTRUCTIONS BEFORE COMPLETING FORM
1. REPORT NUMBER: AFCRL-TR-75-0324	2. GOVT ACCESSION NO. / 3. RECIPIENT'S CATALOG NUMBER
4. TITLE (and Subtitle): POEM: A FAST MONTE CARLO CODE FOR THE CALCULATION OF X-RAY TRANSITION ZONE DOSE AND CURRENT	TYPE OF REPORT & PERIOD COVERED: Scientific Report No. 1 PERFORMING ORG. REPORT NUMBER: SAI-74-624-WA
7. AUTHOR(s): William L. Chadsey	8. CONTRACT OR GRANT NUMBER(s): F19628-73-C-0276
9. PERFORMING ORGANIZATION NAME AND ADDRESS: Science Applications, Incorporated, McLean Virginia 22101	10. PROGRAM ELEMENT, PROJECT, TASK AREA & WORK UNIT NUMBERS: 62704H GDNA0008
11. CONTROLLING OFFICE NAME AND ADDRESS: Air Force Cambridge Research Laboratories, Hanscom AFB, Massachusetts 01731, Contract Monitor: Dr. John C. Garth/LQR	12. REPORT DATE: 15 January 1975 13. NUMBER OF PAGES: -105-
14. MONITORING AGENCY NAME & ADDRESS *(If different from Controlling Office)*: DNA-NATD-QAT; HQ-AF	15. SECURITY CLASS. *(of this report)*: Unclassified 15a. DECLASSIFICATION/DOWNGRADING SCHEDULE

16. DISTRIBUTION STATEMENT *(of this Report)*

Distribution limited to U.S. Government agencies only; Test and Evaluation, Test and Evaluation of Military Systems/Equipment 17 September 1975. Other requests for this document must be referred to AFCRL/LQR, Hanscom AFB, Massachusetts 01731.

17. DISTRIBUTION STATEMENT *(of the abstract entered in Block 20, if different from Report)*

18. SUPPLEMENTARY NOTES

This research was sponsored by the Defense Nuclear Agency under Subtask Z99QAXTA040, Work Unit 51, entitled "Secondary Electron Transport Phenomenology."

19. KEY WORDS *(Continue on reverse side if necessary and identify by block number)*

X-Ray Photoemission; X-Ray Transition Zone Dose; Electron Transport; SGEMP; IEMP; TREE; Monte Carlo.

20. ABSTRACT *(Continue on reverse side if necessary and identify by block number)*

The POEM Monte Carlo electron transport computer code has been developed for the calculation of x-ray photoemission from surfaces and the calculation of x-ray transition zone dose near material interfaces. The x-ray photoemission calculation includes fore and back emission yields, energy spectrum, 1D and 2D angular distributions, 2D and 3D energy-angular distributions, and various moments of the distributions. The x-ray transition zone dose calculation includes 1D energy and charge deposition profiles and 1D energy and charge

DD FORM 1 JAN 73 1473 EDITION OF 1 NOV 65 IS OBSOLETE

UNCLASSIFIED

SECURITY CLASSIFICATION OF THIS PAGE *(When Data Entered)*

deposition profiles and 1D photo-Compton current and energy current profiles. The code has been optimized and Monte Carlo variance reduction techniques have been incorporated to minimize the run time requirements.

The POEM code is described in detail. Applications of the code to x-ray photoemission and transition zone dose are discussed in detail; other applications are briefly discussed. A complete set of user instructions is included.

PREFACE

The CDC computer version of the POEM Monte Carlo code for the calculations of x-ray photoemission and x-ray transition zone dose is now available. The code may be obtained by sending two 2400 foot 1/2 inch reels of magnetic tape to:

General Electric Company - TEMPO
Attention: DASIAC/ESPIG
Post Office Drawer QQ
Santa Barbara
California 93102

The tapes must be accompanied by a letter requesting the code and a distribution approval letter from DNA Headquarters. Approval is obtained by writing to

LTC J.M. Daley (RAEV)
Defense Nuclear Agency
Washington, D.C. 20305

No copy of the POEM code will be released until DNA approval has been obtained.

The development of the POEM code is continuing - revisions continue to be incorporated. Information on coding revisions will be distributed through SAI Technical Notes. Users desiring further information, other versions of the code, or inclusion in the Technical Note distribution should contact the author

W.L. Chadsey
Science Applications, Inc.
1651 Old Meadow Road
McLean
Virginia 22101

ACKNOWLEDGEMENTS

The author wishes to acknowledge the following individuals for valuable contributions to the development of the POEM code: M.J. Berger and S.M. Seltzer of the National Bureau of Standards for ETRAN which provided the basis for the development of POEM; E.T. Kennedy and C. Ragona formerly of the General Electric Company for assistance in developing the early versions of POEM; C.W. Wilson of SAI for the optimization and incorporation of variance reduction techniques; and J.C. Garth and E.A. Burke of the Air Force Cambridge Research Laboratories for their many valuable suggestions.

I wish to thank the Defense Nuclear Agency, the Air Force Cambridge Research Laboratories, and the Harry Diamond Laboratories for the contract support for the development of POEM.

TABLE OF CONTENTS

TABLE OF CONTENTS (Continued)

TABLE OF CONTENTS (Continued)

Section 1

INTRODUCTION

POEM is a FORTRAN code for computing x-ray generated electron currents and depositions in structures. The Monte Carlo method is used for the computation: an electron source distribution is calculated; a large number of electron trajectories are then traced using a random walk procedure, and contributions to currents and depositions are scored for each trajectory. After a large number of electron histories, the contributions are averaged to obtain statistical estimates and standard deviations for the currents and depositions.

The primary applications of the POEM code have been the calculation of x-ray photoemission from surfaces for IEMP (internal electromagnetic pulse) and SGEMP (system-generated electromagnetic pulse) analyses and the calculation of transition zone dose and current for TREE (transient radiation effects on electronics) analyses. These are the applications for which the code was originally developed and for which most interest has been expressed. The procedures for these applications of the code are discussed in detail in this report. Other applications of the POEM code have included analyses of x-ray, γ-ray, and SEM (scanning electron microscope) produced electron currents and depositions in multilayer devices, transient currents and fields in x-ray and electron irradiated dielectrics, induced currents on conductors in x-ray and γ-ray irradiated plated wire memories, and x-ray and γ-ray produced currents and depositions in air near conductor surfaces. These applications

are only briefly discussed in this report; additional information can be obtained from the cited references and from the author.

The POEM code, as stated in the title of this report, is a "fast" Monte Carlo code. This requires some explanation. Over the past several years, a number of transport codes have been developed which are applicable, for example, to the calculation of x-ray photoemission. These include Monte Carlo codes - POEM,[1] SANDYL,[2] ETRAN,[3] and FASTER-BETA[4] - and analytical codes - QUICKE2,[5] EASY1,[6] and BOLT.[7] The Monte Carlo codes are the most rigorous, accurate, and widely applicable. Yet, Monte Carlo codes are in general large, complicated codes which require large amounts of computer core and time to produce predictions containing statistical uncertaintly. Recently, research has concentrated on developing analytical codes which offer the appeal of the more elegant solution, reduced computation cost, and improved precision. Of necessity, however, the analytical codes rely on a number of simplifying approximations. At best, these approximations restrict the applicability of the codes; at worst, they invalidate the predictions through oversimplification. Early codes such as GRAP[8] and EGRESS[9] rely on an invalid rectilinear electron transport model which produces erroneous predictions for back emission yield and fore and back emission angular distributions. While these codes have been known to be in error for some time,[10] their use unfortunately remains common. Later, more sophisticated codes use a truncated Legendre series to represent the electron distribution function. The EASY1 code of Lopez uses a P_1 approximation; the QUICKE2 code of Dellin and MacCallum uses a P_2 approximation. For the conditions for which the code was designed QUICKE2 is an accurate and exceedingly convenient tool.

It must be kept in mind though that its applicability is limited. QUICKE2 predictions disagree with Monte Carlo predictions and experiment for back photoemission yield and fore and back emission angular distributions for photon energies greater than 100 keV.[11] More important, none of the existing analytical codes provide information on the two-dimensional angular distribution of emission for the case of non-normal photon incidence, and none provide information on the dose distribution profile near a material interface.

Rather than abandon the Monte Carlo method and completely embrace the convenient, but limited analytical codes, an alternative course has been pursued. We have built a fast Monte Carlo code for the calculation of x-ray photoemission and transition zone dose and current. We have optimized the POEM Monte Carlo code and incorporated variance reduction techniques such as stratified sampling, importance sampling, track splitting, and control variates which have resulted in an order of magnitude reduction in computation time requirements. For example, for the POEM code calculations of x-ray photoemission presented by Garth and Chadsey,[12] in which comparisons were made with the measurements of Bradford,[13] approximately 15 CP minutes were required on a CDC 6600 to obtain a one percent to two percent standard deviation on the prediction of total yield and five percent to ten percent on the prediction of the emission distributions. This same precision can now be obtained with approximately one CP minute on the CDC 6600.

This dramatic increase in code efficiency has allowed us to perform extensive parametric studies of x-ray photoemission and transition zone dose and current. The emission study included calculations of fore and back emission yield, energy distribution, one- and two-dimensional angular distributions, and the various joint

energy-angular distributions for the elements C, Al, Ti, Cu, Mo, Sn, Ta, and Au, photon energies 0.01, 0.02, 0.05, 0.10, 0.20, 0.50, 1.0, 2.0 MeV and E_K-5 keV where E_K is the K-edge, and photon angles of incidence 0, 30, 60, and 80 degrees with respect to the surface normal. The study also included comparisons of the POEM calculations with QUICKE2 calculations over the range of the parametric study.

The transition zone dose and current parametric study was performed for gold/polyethylene and gold/silicon interfaces for irradiation by monochromatic photon spectra in the range 0.01 to 2.0 MeV. The results include dose and current profiles, contributions due to electron emission and backscatter at the interface, contributions due to the various source electron groups - K and L photoelectrons, K Auger electrons, and Compton electrons - and analytical functional fits to the dose and current profiles.

Extensive computational studies such as the photoemission and transition zone dose and current parametric studies would not have been feasible with the old version of the POEM code or any of the other transport codes, ETRAN, SANDYL, or FASTER-BETA. Computation time requirements would have been excessive. Thus, the conversion of the POEM code to a fast Monte Carlo code has greatly increased its power as a computational tool. To be fair, however, it must be pointed out that the increase in code efficiency could only be obtained through some sacrifice in generality. Codes like SANDYL and FASTER-BETA are large codes applicable to general types of problems. If one wants to make frequent calculations for a problem for which the POEM code was designed, one would be advised to use POEM because of the significant computation cost savings. On the other

hand, for infrequent calculations for complex geometry problems other than those for which POEM was designed, one would be advised to use a code like SANDYL. While we have had little difficulty in adapting POEM to various complex geometries, such as the plated wire memory, this requires familiarity with the code and of course an investment of labor.

Three reports on the POEM code are being published. This report presents the code documentation. The other two reports present the results of the x-ray photoemission and transition zone dose and current parametric studies. The documentation and release of the POEM code should provide the technical community with a convenient and accurate tool for IEMP, SGEMP, and TREE analyses. The results of the x-ray photoemission study should serve to acquaint researchers with the characteristics of electron emission back and fore yields, energy spectra, and one- and two-dimensional angular distributions as functions of material atomic number and photon energy and angle of incidence, and to indicate the ranges of applicability of the analytical codes. The results of the transition zone dose and current study should serve to acquaint researchers with the characteristics of dose and current profiles near high-Z low-Z interfaces and to serve as a data base against which to test future analytical or empirical models.

The POEM code started several years ago as a version of ETRAN which we specialized for the calculation of x-ray photoemission and transition zone dose and current by deleting all procedures extraneous to these calculations. The code has undergone continuous revision since that time. The electron source routines were replaced, the electron multiple scattering distribution calculation was revised, and the random walk, scoring, and output routines were completely

rewritten. Recently, the code was optimized, requiring rewrite of essentially the entire code, variance reduction techniques were incorporated, and fitting routines were added to the transition zone dose and current calculations. Revision of the code has by no means been completed; in fact, at this time we are working on a revolutionary change in the Monte Carlo approach. Documentation and release of the POEM code, however, is long overdue. This report, therefore, describes POEM as of January 1975 - the version used in the parametric studies. In the future, modifications to the code will be described in Technical Notes to be distributed to the users.

Section 2 of this report describes the code applications - problem geometry, range of validity, and computed quantities. Section 3 describes the computational procedures - source generation, history origination, random walk, scoring, history termination, statistical estimation of output quantities and standard deviations, and variance reduction. Section 4 describes the photon and electron cross sections used. Section 5 contains the user instructions and input/output description. The cited references may be found at the end of Section 5. Code listings and sample problems are contained on the master tape along with the program source deck images.

POEM is a family of electron transport codes contained in an UPDATE program library. Each code in the library is designed for a specific application: x-ray photoemission, x-ray transition zone dose, SEM dose, dose and charge deposition in dielectrics, radiation-induced currents in plated wire memories, and so on.

The codes are filed by UPDATE deck name. The deck name for each application is specified in Section 2.

Complete code descriptions are included in Section 2 for the x-ray photoemission and x-ray transition zone dose applications. Brief code descriptions are also included in Section 2 for a number of other applications. Additional information on these codes may be obtained by contacting the author.

Section 2

APPLICATIONS

2.1 X-RAY PHOTOEMISSION: (DECK NAMES 1S1D, 1S2D)

X-rays and γ-rays produce swift Compton, photo-, and Auger electrons in matter. These primary electrons in turn produce secondary, knock-on electrons. Those electrons produced within an electron range from a material surface have a non-zero probability of escaping from that surface. These x-ray and γ-ray generated electron emissions drive IEMP, SGEMP, and source region EMP. Accurate prediction of the IEMP, SGEMP, or source region EMP fields depends on the accurate determination of the yield and energy-angular distribution of the electron emissions. Prediction of electron emission requires calculation of the electron source in the region within an electron range from the emitting surface and the calculation of the electron transport to the surface. POEM uses an analytical model for the source calculation and a Monte Carlo model for the transport calculation.

2.1.1 Problem Geometry

POEM calculates the electron emission from a planar surface. The restriction to planar geometry is not a severe limitation. If the radius of curvature of a surface is large compared with the electron range, the surface effectively appears planar in the transport calculation. Thus, the code can be used to calculate the electron emission for such geometries as spheres, cylinders, and conical sections

provided the radius of curvature is large compared with an electron range. Since, for example, electron ranges in aluminum for 0.01, 0.10, and 1.0 MeV electrons are 0.00013, 0.0069, and 0.20 cm, respectively, this is not a particularly restrictive condition. One exception is the electron emission from a small diameter wire. For this case, a special version of the code has been built as described in Section 2.3

The problem geometry for fore and back emission is defined in Figure 1. The emitting surface of a planar slab of irradiated material lies in the xy-plane; the z-axis lies on the outward normal to the surface. The photons are incident parallel to the xz-plane with angle, θ_o, with respect to the z-axis and with positive direction cosine with respect to the x-axis. POEM calculates the electron emission for the case of plane wave photon irradiation. (For narrow beam photon irradiation, the POEM calculated yields should be multiplied by $\sec\theta_o$.) The photon flux is assumed to be defined at the emitting surface. The POEM code does not calculate the photon flux attenuation within the irradiated material. (The flux attenuation can be easily calculated using any of a number of readily available photon transport codes such as FSCATT[31] or MORSE.[32]) Since the photon flux is assumed to be defined at the emitting surface, the electron emission yield is independent of the slab thickness for thicknesses greater than the maximum electron range. Unless specified, the slab thickness is assumed equal to the maximum electron range. For slab thicknesses thinner than the maximum electron range, the thickness must be specified.

An electron is emitted in direction $\vec{\Omega}$ with angle θ with respect to the z-axis and angle ϕ with respect to the

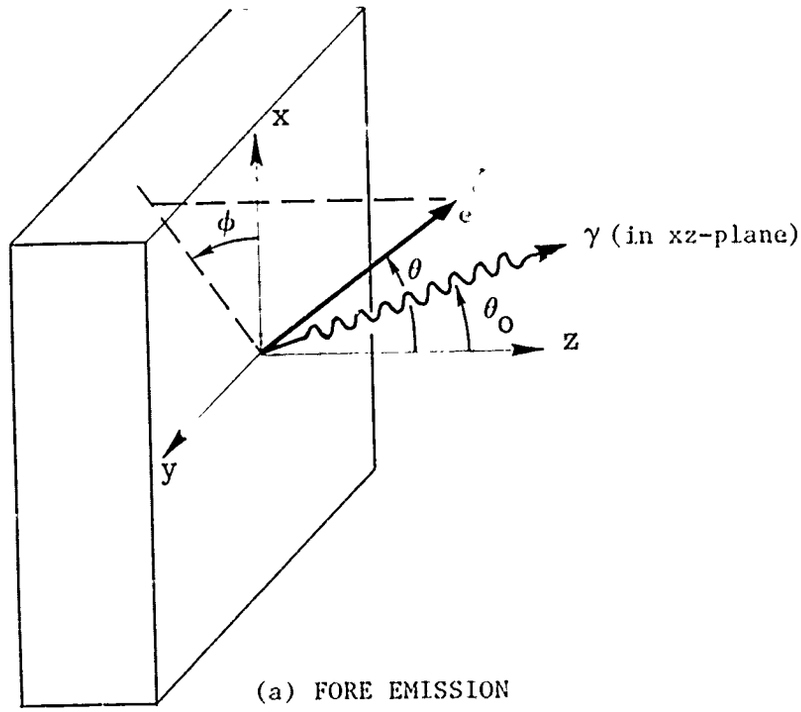

(a) FORE EMISSION

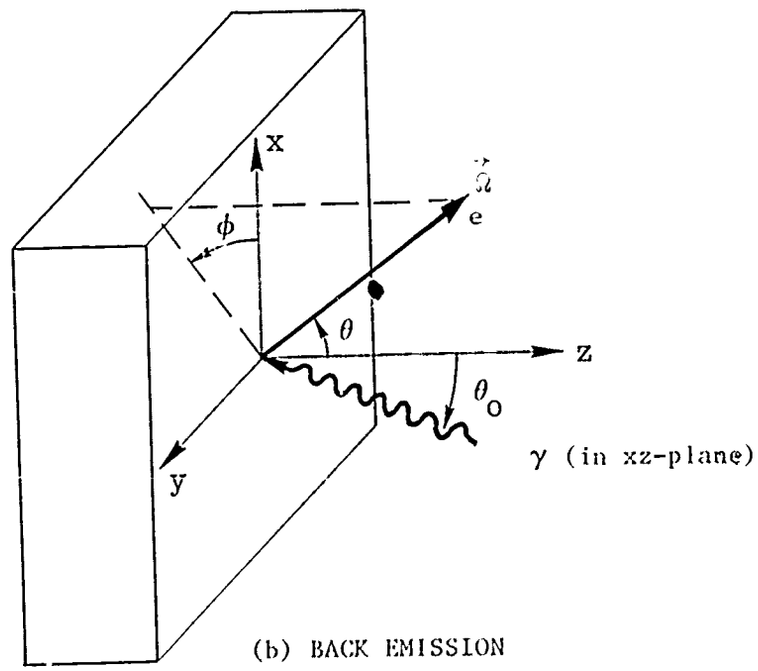

(b) BACK EMISSION

Figure 1

PROBLEM GEOMETRY: X-RAY PHOTOEMISSION

xz-plane. Emission from the slab surface nearer the source is termed back emission (Figure 1b). Emission from the slab surface farther from the source is termed fore emission (Figure 1a).

It is important that the POEM code calculates the full two-dimensional angular distribution of yield $y'(\theta,\phi)$.* The analytical codes EASY1 and QUICKE2 calculate only the one-dimensional angular distribution $y'(\theta)$ which is the full angular distribution integrated over azimuth ϕ. The analytical codes provide no information on the azimuthal distribution of emission for non-normal photon incidence. Knowledge of the full two-dimensional angular distribution is critical to practical IEMP, SGEMP, and source region EMP problems. Consider for example, the SGEMP for a right-circular cylindrical structure irradiated normal to the cylindrical axis by plane wave x radiation (Figure 2). At any point of the irradiated cylindrical surface, except along the line tangential to the wave front, the electron emission angular distribution is asymmetric about the surface normal at that point. At each such point, there is therefore a component of the emission current tangential to the cylindrical surface as well as normal to the surface. This component drives circumferential surface currents on the structure. The analytical codes cannot predict the magnitude of this tangential component of the emission current since they provide no information on the azimuthal angular distribution of electron emission. The POEM code, on the other hand, does predict both the normal and tangential components of the emission current.

---

* Notation: y denotes the total electron yield (electrons/photon); y' denotes a distribution of the yield with respect to one or more variables.

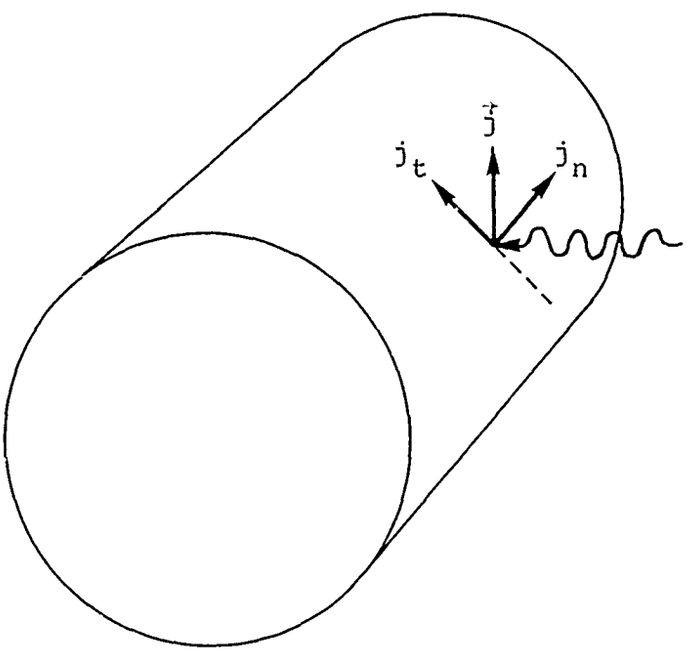

Figure 2

NORMAL AND TANGENTIAL COMPONENTS OF X-RAY PHOTO-EMISSION CURRENT FOR RIGHT-CIRCULAR CYLINDER IR-RADIATED BY PLANE WAVE X-RAYS

2.1.2 Limitations

Photon Environment - The incident photon spectrum can be specified in one of three ways: (1) monochromatic spectrum, (2) black body spectrum, or (3) an arbitrary spectrum defined by up to 120 photon energy groups. The high energy limit for the photon spectrum is 10 MeV. This limitation is principally imposed by the fit used for the radiative energy loss. POEM does not include pair production in the electron source calculation. Because of the positron/electron symmetry of production and near symmetry of transport, the pair production contribution to the emission current is insignificant. For predictions for an emission experiment in which positrons and electrons are distinguishable, however, care must be exercised in using POEM for photon energies greater than several MeV, for which energies pair production constitutes a sizeable fraction of the total photon interaction cross section. The low energy limit for the photon spectrum is determined by the low energy limit for the electron transport. The low energy cutoff on the electron transport is currently 1 keV. A practical low energy limit on the photon spectrum is, then, about 5 keV. While the electron scattering cross sections used are not strictly valid at electron energies as low as 1 keV, in practice we have found reasonable agreement of prediction with experiment for photon energies on the order of 10 keV.

As discussed previously, the photon spectrum is assumed to be defined at the electron emitting surface. For cases in which there is a significant thickness of material between the photon source and the electron emitting surface, the photon intensity and spectrum at the surface must be computed using an appropriate photon transport code.

POEM assumes plane wave photon radiation incident on the electron emitting surface. The POEM predictions, however, are also applicable to narrow beam photon irradiation of the surface provided that the calculated electron yields are multiplied by $\sec\theta_o$, where θ_o is the photon angle of incidence with respect to the surface normal.

The photon angle of incidence with respect to the surface normal is arbitrary, but the incidence must be monodirectional. Extension of the code to accept an angular distribution of photon incidence requires only minor coding changes provided that the photon angular distribution and energy distribution can be assumed to be uncorrelated. Extension to the case of correlated photon angular and energy distributions would require major code modification.

POEM computes both fore and back electron emission for a given photon environment, or if so requested by the user, only fore or back emission.

Material Configuration - The electron emitting material may be any homogeneous material composed of a single element or a composition of up to ten elements. The elements may be any of those for which the photoelectric cross sections are compiled on the ENDF/B file: these are the 87 elements with atomic number Z=1 through 83, 86, 90, 92, and 94.

POEM assumes the electron emitting surface to be planar. The surface geometry may be multidimensional, as discussed previously, provided that the radius of curvature of the surface is large everywhere compared with the maximum electron range.

The electron emission may be calculated for a homogeneous slab of material of arbitrary thickness. If the slab is thick compared with the maximum electron range, the electron yield is independent of thickness, since the photon intensity and spectrum are defined at the emitting surface. The emission may also be calculated for a foil thinner than the maximum electron range, provided that the transport calculation is set up so that the maximum step-size in the random walk is reasonably small compared with the material thickness. If the emitting structure is constructed of several layers of different materials, the surface layer of which is thinner than the electron range, then the emission must be calculated using the multislab version of the code (Section 2.3).

2.1.3 Computed Quantities

The x-ray photoemission quantities computed by POEM are summarized in Table 1. All quantities shown in this table are computed for both fore and back emission. The total yield y is expressed in electrons/photon, coul/cal(photons) and cal(electrons)/cal(photons). If $y'(E,\theta,\phi)$ is the distribution of yield per unit electron energy, per unit solid angle, per incident photon, the calculated total yield is

$$y = \int_{E_{min}}^{E_{max}} dE \int_{0}^{2\pi} d\phi \int_{0}^{\pi/2} d\theta \, \sin\theta \, y'(E,\theta,\phi) \qquad (1)$$

where E_{min} = 1 keV is the minimum electron energy and $E_{max} \leq h\nu_{max}$ is the maximum electron energy and $h\nu_{max}$ is the maximum photon energy.

Table 1 COMPUTED QUANTITIES: X-RAY PHOTOEMISSION

QUANTITY	UNITS	COMMENTS
y, yield	(1) electrons/photon (2) coulombs/calorie(photon) (3) calorie(electron)/ calorie(photon)	(1) all quantities are calculated for both fore and back emission (2) standard errors are calculated for all quantities
$y'(\theta)$, polar angular distribution of yield	(1) electrons/photon-Sr (2) electrons/photon-deg	
$y'(\varphi)$, azimuthal angular distribution of yield	electrons/photon-deg	
y'(E), energy spectrum of yield	electrons/photon-keV	
$y'(\theta,\phi)$, two-dimensional angular distribution of yield	electrons/photon-Sr	two- and three-dimensional distributions of yield are written on TAPE13 rather than on OUTPUT
two- and three-dimensional distributions of yield: $y'(E,\theta)$ $y'(E,\phi)$ $y'(E,\theta,\varphi)$	electrons/photon-Sr-keV	

Table 1 (Continued)

QUANTITY	UNITS	COMMENTS
Moments of yield distributions:		
$\langle E \rangle$, mean energy	keV	
$\langle \vartheta \rangle$, mean angle with respect to surface normal	degrees	
$\langle \cos\theta \rangle = \langle \vec{\Omega} \cdot \hat{z} \rangle$, mean direction cosine with respect to z-axis		
$\langle \sin\theta\cos\phi \rangle = \langle \vec{\Omega} \cdot \hat{x} \rangle$, mean direction cosine with respect to x-axis		
Components of emission current:		
J_z, current normal to surface	electrons/photon	(1) plane wave photon incidence assumed
J_x, current tangential to surface	electrons/photon	(2) $J_z = y$
		(3) for $\vartheta_o = 0$, $J_x = 0$.

Table 1 (Continued)

QUANTITY	UNITS	COMMENTS
Electron source parameters:		
S, source density	electrons/photon	photon-generated source density in source region
S'(θ), angular distribution of source with respect to photon direction	electrons/photon-Sr	optional outputs
S'(E), energy distribution of source	electrons/photon-keV	
S'(E,θ), two-dimensional source distribution	electrons/photon-Sr-keV	
Transport diagnostics:		
(1) number of particle histories		
(2) number of particle emissions		
(3) mean number of transport steps per emission		
(4) mean angular deflection per emission		
(5) mean probability of emission from source region		

The various emission distribution functions are expressed both in absolute units and normalized to the total yield. The one-dimensional distribution functions are defined as

$$y'(E) = \int_0^{2\pi} d\phi \int_0^{\pi/2} d\theta \sin\theta \, y'(E,\theta,\phi) \tag{2}$$

$$y'(\theta) = \int_0^{2\pi} d\phi \int_{E_{min}}^{E_{max}} dE \, y'(E,\theta,\phi) \tag{3}$$

$$y'(\phi) = \int_0^{\pi/2} d\theta \int_{E_{min}}^{E_{max}} dE \, y'(E,\theta,\phi) \tag{4}$$

Note that the polar angular distribution is expressed both as the electron yield per unit solid angle $y'(\theta)$ and as the electron yield per unit scattering angle $y''(\theta) = 2\pi \sin\theta \, y'(\theta)$.

The two-dimensional distribution functions are defined as

$$y'(E,\theta) = \int_0^{2\pi} d\phi \, y'(E,\theta,\phi) \tag{5}$$

$$y'(E,\phi) = \int_0^{\pi/2} d\theta \sin\theta \, y'(E,\theta,\phi) \tag{6}$$

$$y'(\theta,\phi) = \int_{E_{min}}^{E_{max}} dE\ y'(E,\theta,\phi) \qquad (7)$$

The normal maximum resolution for the electron emission distribution functions is 20 energy bins, 10 θ-angle bins, and 8 ϕ-angle bins. Resolution can be increased through increasing the dimensions of the code, as for example was done in the calculations reported by Garth and Chadsey.[12]

Several moments of the emission distribution are also calculated. These include the mean emitted electron energy $\langle E \rangle$, the mean cosines of the polar angular and azimuthal angular distributions, $\langle \cos\theta \rangle$ and $\langle \cos\phi \rangle$, and $\langle \sin\theta\cos\phi \rangle$. The $\langle \cos\theta \rangle$ is a measure of how strongly the emission solid angular distribution is directed in the direction of the outward normal to the surface. The $\langle \cos\phi \rangle$ and $\langle \sin\theta\cos\phi \rangle$ are measures of the asymmetry of the azimuthal angular distribution due to oblique photon incidence. (For normal photon incidence $\langle \cos\phi \rangle$ and $\langle \sin\theta\cos\phi \rangle$ are zero.)

Since POEM is a Monte Carlo code, the computed emission quantities are statistical estimates of the emission parameters. It is therefore important not only to calculate the desired quantities but also to estimate the statistical precision of the calculations. For each of the electron emission quantities discussed above, POEM calculates the estimated standard deviation.

In addition to these electron emission quantities, POEM calculates several quantities describing the electron source and the electron transport. The source parameters

are the source density S in electrons/photon (averaged over the source region), the source energy spectrum S'(E), the source angular distribution with respect to the photon direction S'(θ), and the two-dimensional source distribution S'(E,θ). Also calculated are the mean source electron energy and the maximum energies of the Compton electrons, K and L photoelectrons, and K-Auger electrons. The transport parameters are the average number of random walk steps and average total deflection of the particles which escape the surface, the total number of particles which escape the surface, and the mean probability of escape for the source electrons.

Two versions of the emission code exist: one for the calculation of the two-dimensional angular distribution y'(θ,ϕ) (deck name 1S2D); the other for only a one-dimensional calculation y'(θ) (deck name 1S1D). For cases of normal photon incidence or for which the two-dimensionality of the emission distribution is not of concern, the one-dimensional version should be used since it is significantly faster.

2.2 TRANSITION ZONE DOSE AND CURRENT: (DECK NAME 2S)

Dose is defined by the International Commission on Radiological Units (ICRU) as the energy imparted to matter by ionizing radiation per unit mass of matter. The "energy imparted to matter" is that which appears as ionization or excitation, increase in crystal-lattice energy, and so forth in the material. This is just that energy removed from the radiation field as a whole. For γ-ray or x-ray irradiation of matter, the radiation field consists of the primary photons and secondary photons, and the photo-Compton and secondary electrons. In a region of a homogeneous material far from the photon source and farther from any interface with a dissimilar material than the range of the

most penetrating of the electrons, electron equilibrium exists: the energy transported into an incremental volume of matter by electrons is equal in the mean to the energy transported out of the volume by electrons. The equilibrium dose is thus equal to the energy removed from the photon radiation field per unit mass of matter - the kerma. The equilibrium dose can be determined directly from calculation of the photon transport; the electron transport need not be calculated.

Near a boundary between dissimilar materials electron equilibrium fails because of differences in the electron production and transport properties of the different materials. The energy transported into an incremental volume of matter by electrons is not equal to the energy transported out by electrons. Thus the dose is not equal to the kerma. Since in general the energy directly imparted to the matter by the primary photons is negligible compared with the energy imparted by the electrons, the dose is critically sensitive to the electron balance. Nonequilibrium dose can differ from the kerma by more than an order of magnitude.

In a region of a x-ray or γ-ray irradiated material in which electron equilibrium exists, the photo-Compton current is proportional to the photon flux. The constant of proportionality is a function of the photon energy and the atomic number of the material, but is independent of the material density or spatial location within the material. Near the boundary between dissimilar materials, this relationship breaks down because of the failure of electron equilibrium. The nonequilibrium photo-Compton current, just as the dose, may differ significantly from the equilibrium value. The divergence in electron current near a

boundary between dissimilar materials results in charge deposition near the boundary.

The region near a material interface in which electron equilibrium fails is known as the transition zone. The dose and current distributions in the transition zone are referred to variously as transition zone dose and current, non-local charge and energy deposition, and dose enhancement. Transition zone dose and current effects are important in weapons radiation effects problems such as TREE, IEMP in cables, and charge buildup in dielectrics, as well as in problems in radiography and radiology. The POEM code provides a convenient, accurate tool for the analysis of transition zone dose and current.

2.2.1 Problem Geometry

POEM calculates the transition zone dose and current in the region within an electron range from planar interface between two materials irradiated by plane wave x or γ radiation. The problem geometry is defined in Figure 3. The planar interface between materials A and B lies in the xy-plane. The z-axis is directed away from material A. The plane wave photon radiation is incident at an angle θ_o with respect to the z-axis. The photon incidence can be either through material A or B. Just as with the emission code, the photon intensity and spectrum are assumed to be defined at the interface. A and B are planar slabs of arbitrary thickness. N deposition zones of of thickness Δz are defined in B by planes parallel to the interface at distances $z_1 = \Delta z$, $z_2 = 2\Delta z$, ..., $z_N = N\Delta z$. The photo-Compton charge and energy currents are calculated at the planes $z = 0, z_1, z_2, \ldots, z_N$. The charge and energy deposition are calculated in the N zones.

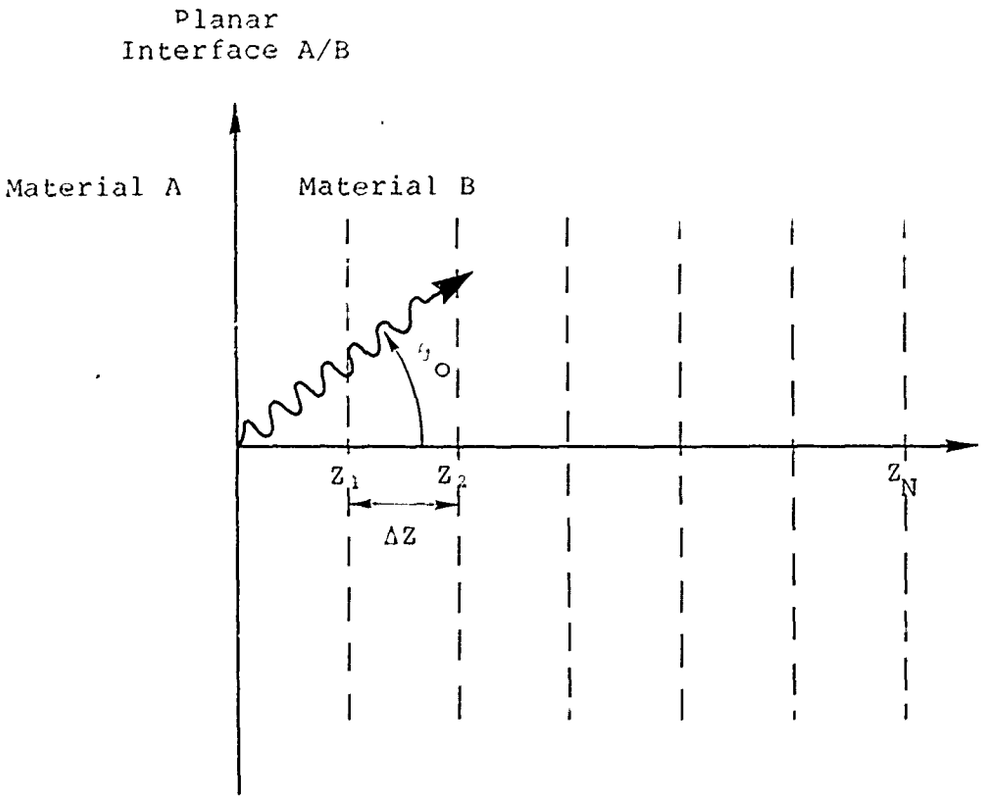

Figure 3

PROBLEM GEOMETRY: TRANSITION ZONE DOSE CURRENT

2.2.2 Limitations

Photon Environment - The transition zone dose and current calculation is valid for photon energies in the range 5 keV$\leq h\nu \leq$2 MeV. The lower limit is determined by the 1 keV cutoff on the electron transport. The upper limit is determined by the exclusion of pair production in the electron source calculation. While pair production does not significantly contribute to the photo-Compton current because of particle/antiparticle symmetry, pair production does significantly contribute to dose for $h\nu \geq$2 MeV.

The calculation assumes plane wave photon radiation. The angle of incidence with respect to the normal to the interface can be $0 \leq \theta_o \leq 1^{\circ}0^{\circ}$. Just as in the emission calculation, the code can easily be modified to accept an angular distribution of photon incidence, provided that the photon energy and angular distributions can be assumed to be uncorrelated.

The photon intensity and spectrum are assumed to be defined at the material interface. If these are unknown, then the flux attenuation between the photon source and the interface must be calculated using an appropriate photon transport code.

Material Configuration - The code calculates the transition zone dose and current in the neighborhood of a planar interface between two materials. The materials may be any of those materials for which the emission code can be used. The code normally sets the material thicknesses equal to the maximum electron range in each material. Since the photon flux is assumed to be defined at the interface, increasing the material thicknesses beyond the

maximum electron ranges does not affect the results. The minimum material thicknesses are determined by the step sizes selected for the transport calculation. The deposition zone width should be larger than the longest step size of the random walk.

2.2.3 Computed Quantities

The calculated transition zone dose and current quantities are summarized in Table 2. The current and deposition distributions are calculated in material B as functions of the distance z from material A, over the region from the interface out to the maximum electron range. The distributions are the photo-Compton current per unit photon flux (electrons/photon), the photo-Compton energy flux per unit photon energy flux (dimensionless), the charge deposition density per unit photon flux (electrons/g)/(photon/cm^2), the dose per unit photon energy fluence (cm^2/g), and the relative dose (the ratio of dose to kerma, which is dimensionless).

In addition to the dose and current profiles, the electron yield y at the interface and the energy distribution y'(E) and angular distribution y'(θ) with respect to the interface normal are calculated. For the case of the electrons arising in the deposition material (material B), the yield y is the backscatter yield. For the case of the electrons arising in the neighboring material (material A), the yield y is the emission yield.

Separate calculations are made of the contributions to the dose and current profiles due to (1) emission of electrons across the interface and (2) backscatter of electrons from the interface. Separation of the emission and backscatter components of the profiles is useful to

Table 2 COMPUTED QUANTITIES: X-RAY TRANSITION ZONE DOSE

QUANTITY	UNITS	COMMENTS
$J_z(z)$, z-component of photo-Compton current	electrons/photon	standard deviations are calculated for all quantities
$G_z(z)$, z-component of electron vector energy fluence	calories(electron)/calorie(photon)	
Q(z), electron charge deposition	(electrons/g)/(photon/cm^2)	
D'(z), nonequilibrium component of dose	(cal/g)/(cal(photon)/cm^2) = cm^2/g	(1) dose D = D'+K, where K = kerma (equilibrium dose) (2) relative dose (dose/kerma) R = 1+D'/K
Fit coefficients: A,B,C,D for $J_z(z)$	z in g/cm^2	$J_z(z) \underset{\sim}{\sim} A\exp(Bz+Cz^2+Dz^3)$
A,B,C,D for $G_z(z)$ and D'(z)		$G_z(z) \underset{\sim}{\sim} A\exp(Bz+Cz^2+Dz^3)$ $D'(z) = -\frac{dG_z}{dz}$ $\underset{\sim}{\sim} A(B+2Cz+3Dz^2)\exp(Bz+Cz^2+Dz^3)$

Table 2 (Continued)

QUANTITY	UNITS	COMMENTS
Interface parameters:		
y, yield at interface	(1) electrons/photon	(1) for electron source in deposition material, y = backscatter yield
	(2) cal(electrons)/cal(photon)	(2) for electron source in neighboring material, y = emission yield
y'(E), energy spectrum of yield	electrons/photon-keV	
y'(θ), angular distribution of yield with respect to normal to interface	electrons/photon-Sr	
Source parameters: (same as in Table 1)		
Transport parameters: (same as in Table 1)		

understanding the interface effects. Furthermore, the efficiency of the Monte Carlo calculation is increased through the separation of the components and the proper allocation of the Monte Carlo histories to the separate calculations, as discussed in Section 3.2.

Separate calculations can also be made of the contributions to the current and dose profiles due to electrons from each of the source groups: Compton, K-photo, L-photo, and K-Auger electrons. This separation is again useful to the interpretation of the interface effects. It can also be used to increase code efficiency and to increase the resolution of the dose and current profiles.

The Monte Carlo output is in the form of the charge and energy currents at each plane bounding the deposition zones and charge and energy deposition within each deposition zone. In addition to the Monte Carlo data, the code calculates coefficients for analytical functions to fit the Monte Carlo data. The purpose of the functional representation of the data is twofold: first, to provide useful expressions to describe the profiles, and second, to smooth out statistical fluctuations in the Monte Carlo data. The computed charge and energy current profiles are fitted to functions of the form

$$y(x) = A \exp(Bx + Cx^2 + Dx^3) \qquad (8)$$

The expressions for the charge and energy deposition profiles are determined through analytical differentiation of the functions.

2.3 SPECIAL PURPOSE CODES

In addition to the emission code and interface code described above, several other special purpose POEM codes have been developed. These codes are basically the same as the previous codes, generally differing only in the random walk and result subroutines. The applications of these codes are described briefly in the following paragraphs. The user instructions for these codes are not included in this report, nor are the appropriate subroutines included in the released POEM library. The instructions and routines, however, may be obtained from the author.

2.3.1 Multislab Transition Zone Dose and Current: (MS)

This code calculates the photo-Compton current and dose profiles through a stack of thin foils, each foil thinner than the maximum electron range. The problem geometry is defined in Figure 4. A stack of up to 20 planar slabs of up to four different materials is exposed to plane wave photon radiation incident at an angle θ_o with respect to normal to the slabs. The configuration is zoned into up to 100 deposition zones. The photo-Compton charge and energy current and deposition profiles are calculated. Sample results are included in Reference 14.

2.3.2 Scanning Electron Microscope Dose and Current: (SEM)

This code calculates the two-dimensional current and dose profiles in a one to three layer structure irradiated by the electron beam of a scanning electron microscope (SEM). The problem geometry is defined in Figure 5. A structure composed of up to three thin, planar slabs of material is normally irradiated by a narrow electron beam. The code uses a cylindrical coordinate system with the z-axis along

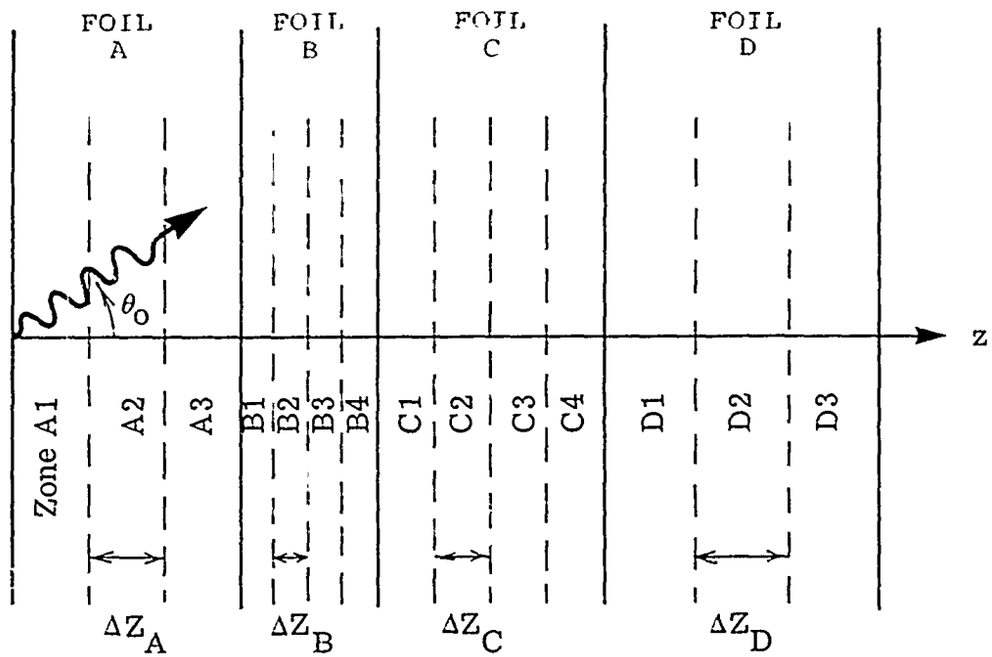

Figure 4

PROBLEM GEOMETRY: MULTISLAB TRANSITION ZONE DOSE AND CURRENT

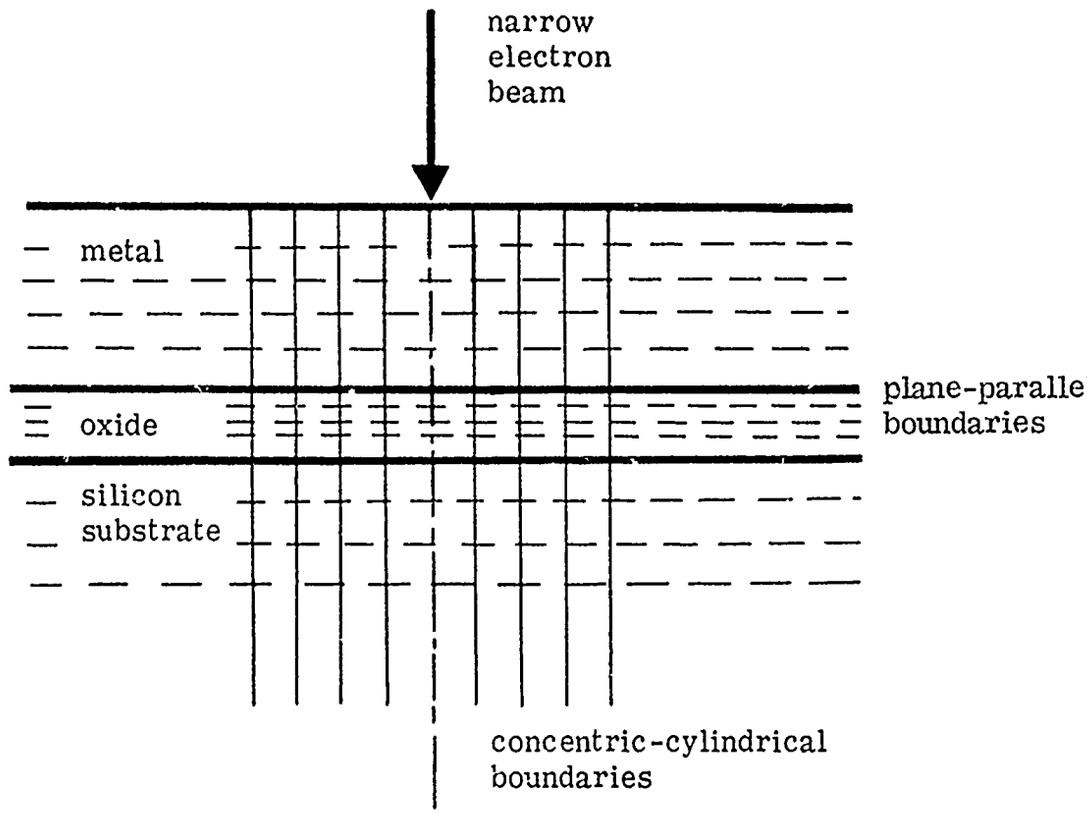

Figure 5

PROBLEM GEOMETRY: SEM CURRENT AND DOSE

the electron beam. The code calculates the two-dimensional current and dose distributions, $j(r,z)$ and $D(r,z)$, the backscattered charge and energy, and the radial distribution of the backscattered electrons. A discussion of the code and sample results for MOS devices are included in Reference 15.

2.3.3 Transition Zone Dose and Current in Dielectrics: (DIEL)

This code calculates the transition zone dose and current in an x- or γ-irradiated dielectric near a planar interface. The electron transport calculation includes the electron acceleration in the electric field of the trapped charge in the dielectric. The time-dependent field calculation includes a time-dependent, spatially-dependent treatment of the transient conduction currents in the dielectric. The problem geometry is shown in Figure 6. A planar interface between a conductor and dielectric is exposed to plane wave x or γ radiation. The xy-plane lies along the interface; the z-axis is directed into the dielectric. The code calculates the photo-Compton current $j(z,t)$, the true current $J(z,t)$,

$$J(z,t) = j(z,t) + \sigma(z,t)\ E\ (z,t) \tag{9}$$

the charge density

$$\rho(z,t) = -\int_0^t \frac{\partial J}{\partial z}\, dt' \tag{10}$$

the radiation-induced conductivity $\sigma(z,t)$, and the electric field $E(z,t)$.

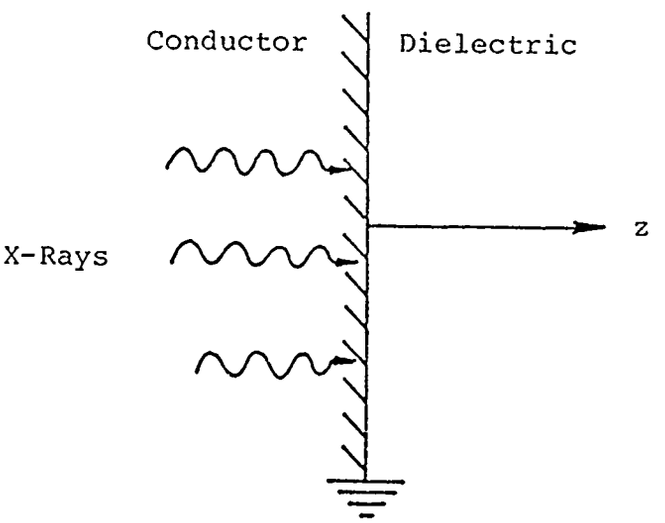

Figure 6

PROBLEM GEOMETRY: TRANSITION ZONE DOSE AND CURRENT IN DIELECTRICS

A discussion of the dielectric code and sample results are found in Reference 16. The code is presently being modified to treat a planar conductor/dielectric/conductor sandwich configuration. It is planned to build a three-dimensional version of this code within the next year.

2.3.4 IEMP in a Plated Wire Memory: (PWM)

A three-dimensional version of POEM was developed for the calculation of the induced bit wire and word strap currents in a plated wire memory exposed to x or γ radiation. The electron transport is calculated for the problem geometry defined in Figure 7. The charge displacement in the memory structure is translated into induced currents on the bit wires and word straps using a Green's function computational technique. The coupling is represented by equivalent current sources driving a lumped element circuit representation of the memory electrical configuration.

2.3.5 Compton Currents in a Right Circular Cylinder

A two-dimensional version of POEM was developed for the calculation of the Compton currents and gas ionization in a gas-filled right circular cylinder irradiated end-on by photons (Figure 8). The two-dimensional distributions of the axial and radial space current components and the energy deposition in the gas are calculated for an arbitrary incident photon energy-angular distribution. The electron sources include the front, back and side walls of the cylinder, the gas, and an optional, coaxial inner cylinder. Space-charge limitation is negligible for the application for which the code was designed, so self-consistent effects are ignored in the transport calculation. These transport

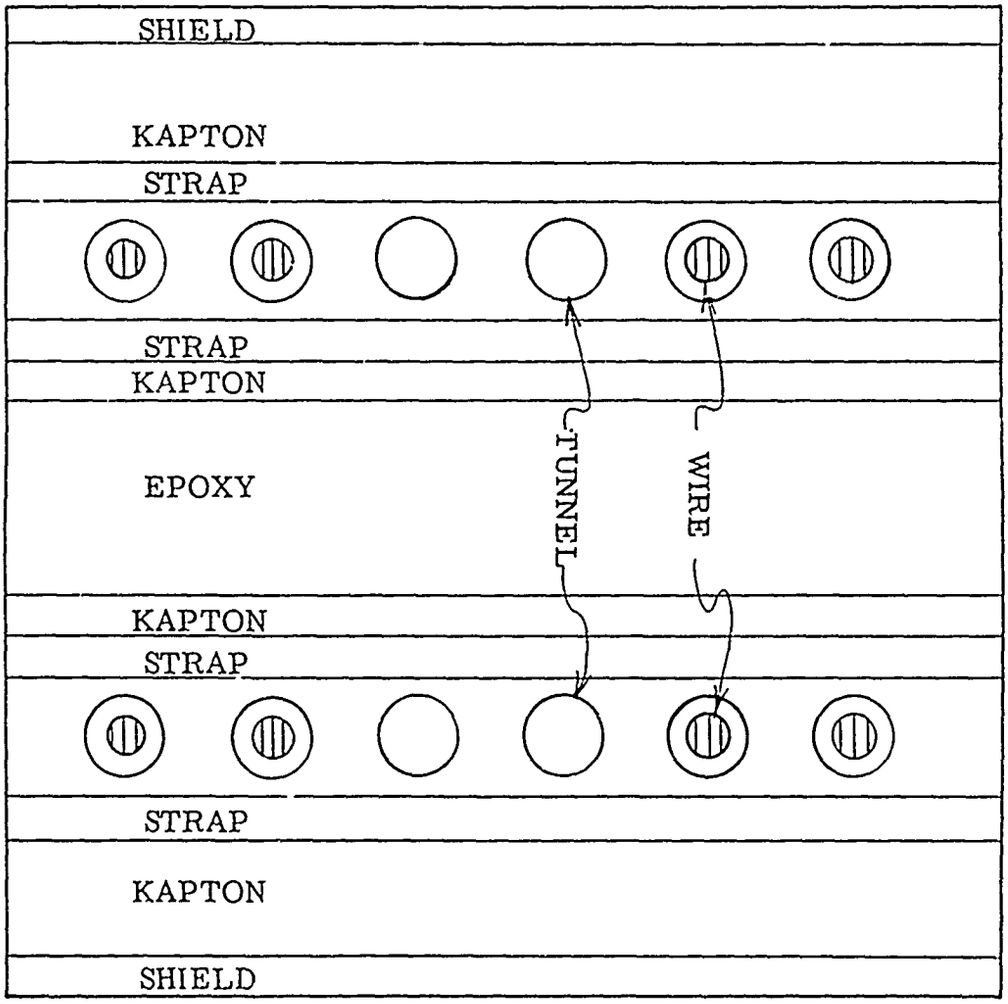

Figure 7

PROBLEM GEOMETRY - PLATED WIRE MEMORY

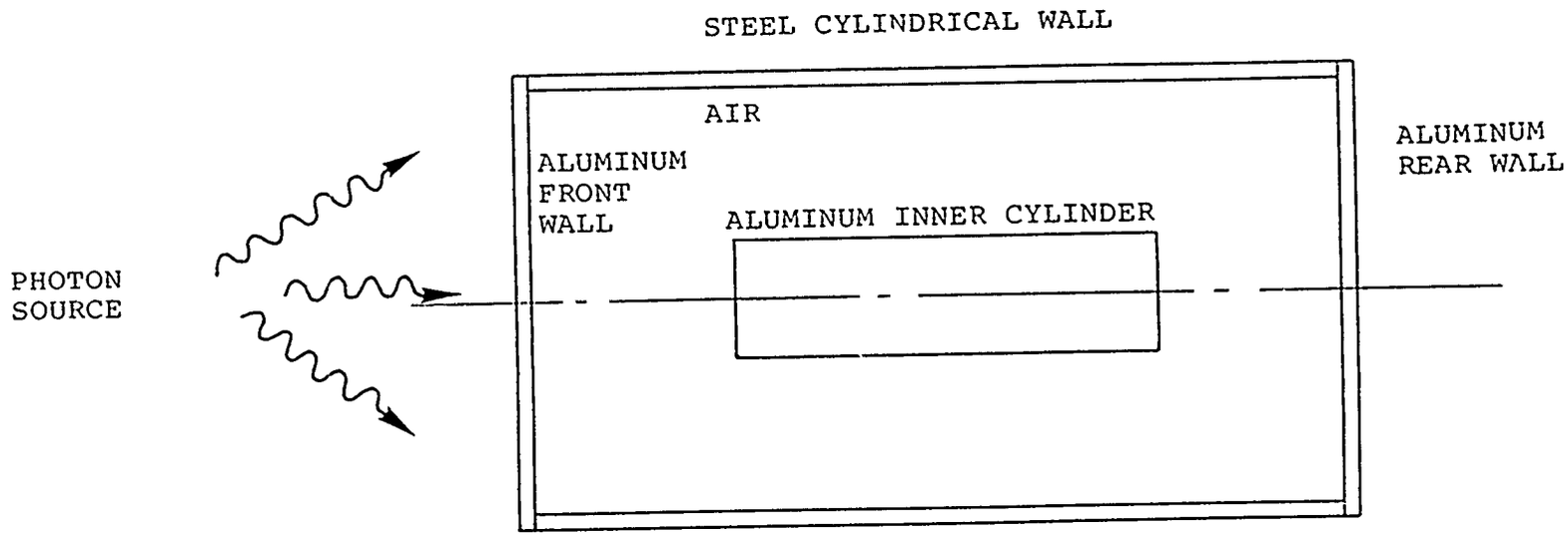

Figure 8

PROBLEM GEOMETRY - CYLINDRICAL CAVITY

calculations are used as inputs to a source region EMP code for the calculation of the fields within the cavity and the surface current induced on the inner cylinder. The code and sample calculations are discussed in Reference 29.

Section 3

COMPUTATIONAL PROCEDURES

The computation of the x-ray photoemission or the transition zone dose and current involves three main parts: (1) calculation of the photon-generated electron source distribution, (2) calculation of the electron transport, and (3) processing of the transport data to obtain the results. In the following paragraphs the computational procedures used in each of these calculations are discussed. In order to efficiently provide an overview of these procedures, detailed discussion of the cross sections employed in the calculations is postponed until Section 4.

3.1 ELECTRON SOURCE CALCULATION

The calculation of the photon-generated electron source distribution is performed using an analytical model. To do this, it is assumed that (1) the photon flux (intensity and spectrum) is defined at the emission surface (or material interface), and (2) the photon flux is constant over the region of the material within an electron range from the surface. This means that it is assumed that the maximum electron range is small compared to the photon mean-free path,

$$r_e << \frac{1}{\mu}$$

a good assumption for the range of applicability of the code. In this approximation the electron source density is constant

over the region contributing to the electron emission. We call this region the source region.

Let the thickness of the electron source region be $\Delta z(g/cm^2)(\Delta z \leq r_e)$, and the planar fluence of the photon group of energy $h\nu$ by $\gamma(h\nu)(photons/cm^2)$. For a Compton cross section $\sigma_{inc}(cm^2/g)$, the density $S_C(electron/cm^2)$ of Compton electrons produced in the source region by photons of energy $h\nu$ is

$$S_C(h\nu) = \gamma\sigma_{inc}\,\Delta z \tag{11}$$

For a photoelectric cross section σ_τ, the density of photoelectrons is

$$S_\tau(h\nu) = \gamma\sigma_\tau\Delta z \tag{12}$$

For each photon energy group, the source calculation includes two photoelectron energy groups as defined in Table 3 where E_K is the K photoelectric absorbtion edge and $E_{\overline{L}}$, $E_{\overline{M}}$, and $E_{\overline{N}}$ are the mean L, M, and N edges.

The mean edges and the relative probabilities for that shell in which the ionization occurs have been calculated using the ratios of the photoelectric cross sections just below and just above the absorbtion edge. The photoelectric cross section undergoes a jump at each atomic shell binding energy E_b (edge). The ratio of the cross section just below the edge E_b to the cross section just above the edge is the probability that the ionization occurs in one of the shells with binding energy less than E_b. We make the common assumption[19] that this probability is constant for all photon energies between E_b and the next larger shell binding energy. For example, for $h\nu \geq E_K$ the probability

Table 3

PHOTOELECTRON ENERGY GROUPS

PHOTON ENERGY	PHOTOELECTRON GROUP	RELATIVE PROBABILITY	PHOTOELECTRON ENERGY
$E_K \leq h\nu$	K	$1-r_K$	$h\nu-E_K$
	L	r_K	$h\nu-E_{\overline{L}}$
$E_{\overline{L}} \leq h\nu < E_K$	L	$1-r_{L_1}r_{L_2}r_{L_3}$	$h\nu-E_{\overline{L}}$
	M	$r_{L_1}r_{L_2}r_{L_3}$	$h\nu-E_{\overline{M}}$
$E_{\overline{M}} \leq h\nu < E_{\overline{L}}$	M	$1-r_{M_1}r_{M_2}r_{M_3}r_{M_4}r_{M_5}$	$h\nu-E_{\overline{M}}$
	N	$r_{M_1}r_{M_2}r_{M_3}r_{M_4}r_{M_5}$	$h\nu-E_{\overline{N}}$

that the ionization occurs in the L shell or lower binding energy shell is r_K where r_K is the ratio of the cross sections just above and just below the K edge. The probability that the ionization occurs in the K shell is $1-r_K$. We use only two photoelectron groups; we lump the L and lower binding energy shell ionizations together by defining the relative K and L shell ionization probabilities to be

$$p_K = 1 - r_K \tag{13}$$

$$p_L = 1 - p_K = r_K \tag{14}$$

for $h\nu \geq E_K$.

Similarly for $E_{\overline{L}} < h\nu < E_K$ we define

$$p_M = 1 - r_{L_1} r_{L_2} r_{L_3} \tag{15}$$

$$p_{L_1} = 1 - r_{L_1} \tag{16}$$

$$p_{L_2} = r_{L_1}(1-r_{L_2}) \tag{17}$$

$$p_{L_3} = r_{L_1} r_{L_2}(1-r_{L_3}) \tag{18}$$

where r_{Li} is the cross section ratio at the L_i edge. We lump the three L subshell ionizations together by defining a relative L shell ionization probability,

$$p_L = p_{L_1}+p_{L_2}+p_{L_3} = r_{L_1} r_{L_2} r_{L_3} \tag{19}$$

and a mean L edge,

$$E_{\bar{L}} = \frac{1}{p_L} \sum_{i=1}^{3} p_{Li} E_{Li} \tag{20}$$

The mean L edge is used in calculation of the L photoelectron kinetic energy as shown in Table 3. Similarly, for $E_{\bar{M}} < h\nu < E_{\bar{L}}$ we define relative ionization probabilities p_M and p_N and a mean M edge $E_{\bar{M}}$:

$$p_M = \sum_{i=1}^{5} p_{Mi} \tag{21}$$

$$E_{\bar{M}} = \frac{1}{p_M} \sum_{i=1}^{5} p_{Mi} E_{Mi} \tag{22}$$

where

$$p_{Mi} = r_{M_1} r_{M_2} \cdots r_{Mi-1} (1 - r_{Mi}) \tag{23}$$

The photoelectron source group definition is summarized in Table 3. The mean N edge is approximated by zero. The code is invalid for $h\nu < E_{\bar{M}}$ ($E_{\bar{M}} < 5$ keV). The relative ionization probabilities defined in Table 3 and the mean edges defined in Equations (20) and (22) have been precalculated and stored on the photon interaction data tape.

Following the photoelectric ionization the atom will relax emitting either a fluorescent photon or an Auger

electron. For the electron source calculation, one Auger electron energy group is included for each photon energy group as defined in Table 4. The K shell fluorescence yield $\bar{\omega}_L$ have been obtained from the Storm and Israel[19] and Bambynek, et al.[25] compilations, with preference given to the Bambynek compilation, and stored on the photon interaction data tape. The mean M fluorescence yield $\bar{\omega}_M$ is approximated by zero.

The total electron source density S'(hν) produced by the photon group of energy hν is the sum of the Compton, photoelectric, and Auger electrons,

$$S'(h\nu) = S_C(h\nu) + S_\tau(h\nu) + S_A(h\nu) \tag{24}$$

The total source density S is obtained by summing S'(hν) over the photon spectrum:

$$S = \sum_{i=1}^{120} S'(h\nu_i) \tag{25}$$

The photon spectrum is defined in the code as (1) a monochromatic spectrum, (2) a black body spectrum internally calculated over 120 photon energy groups, or (3) an arbitrary spectrum defined over up to 120 photon energy groups. The spectrum is internally normalized to a planar fluence of 1 photon/cm^2.

The energy-angular distributions of the Compton, photo-, and Auger electrons are calculated using the cross sections discussed in Section 4. These distributions are summed over the photon spectrum to obtain a joint energy-angular distribution function for the electron source.

Table 4

AUGER ELECTRON ENERGY GROUPS

PHOTON ENERGY	AUGER ELECTRON GROUP	PROBABILITY	ENERGY
$E_K \leq h\nu$	K	$(1-\omega_K)P_K$	$E_K - 2E_{\bar{L}}$
$E_{\bar{L}} \leq h\nu < E_K$	L	$(1-\bar{\omega}_L)P_L$	$E_{\bar{L}} - 2E_{\bar{M}}$
$E_{\bar{M}} \leq h\nu < E_{\bar{L}}$	M	P_M	$E_{\bar{M}}$

This is a discrete distribution function defined over a two-dimensional array of 20 energies by 20 angles. The function is stored as an array $H(E_i,\theta_j)$, i=1,20, j=1,20 where

$$H(E_i,\theta_j) = p(E_1) + p(E_2) + \ldots + p(E_{i-1}) + p(E_i)[p(\theta_1|E_i) + p(\theta_2|E_i) + \ldots + p(\theta_j|E_i)] \quad (26)$$

where

$$p(E_i) = \text{prob}\left\{E_i - \frac{\Delta E}{2} < E \leq E_i + \frac{\Delta E}{2}\right\}$$

and

$$p(\theta_j|E_i) = \text{prob}\left\{\theta_j - \frac{\Delta\theta}{2} < \theta \leq \theta_j + \frac{\Delta\theta}{2} \;\middle|\; E_i - \frac{\Delta E}{2} < E \leq E_i + \frac{\Delta E}{2}\right\}$$

The angular distribution is calculated with respect to the photon direction of incidence (Figure 9). The polar angular (θ) distribution is defined over 0 to π. The azimuthal angular (ϕ) distribution about the direction of photon incidence is assumed to be uniform over 0 to 2π. In addition to the joint, cumulative distribution function, the marginal (one-dimensional) energy and angular distribution functions $p(E_i)$ and $p(\theta_i)$, i=1,20, are calculated for the output.

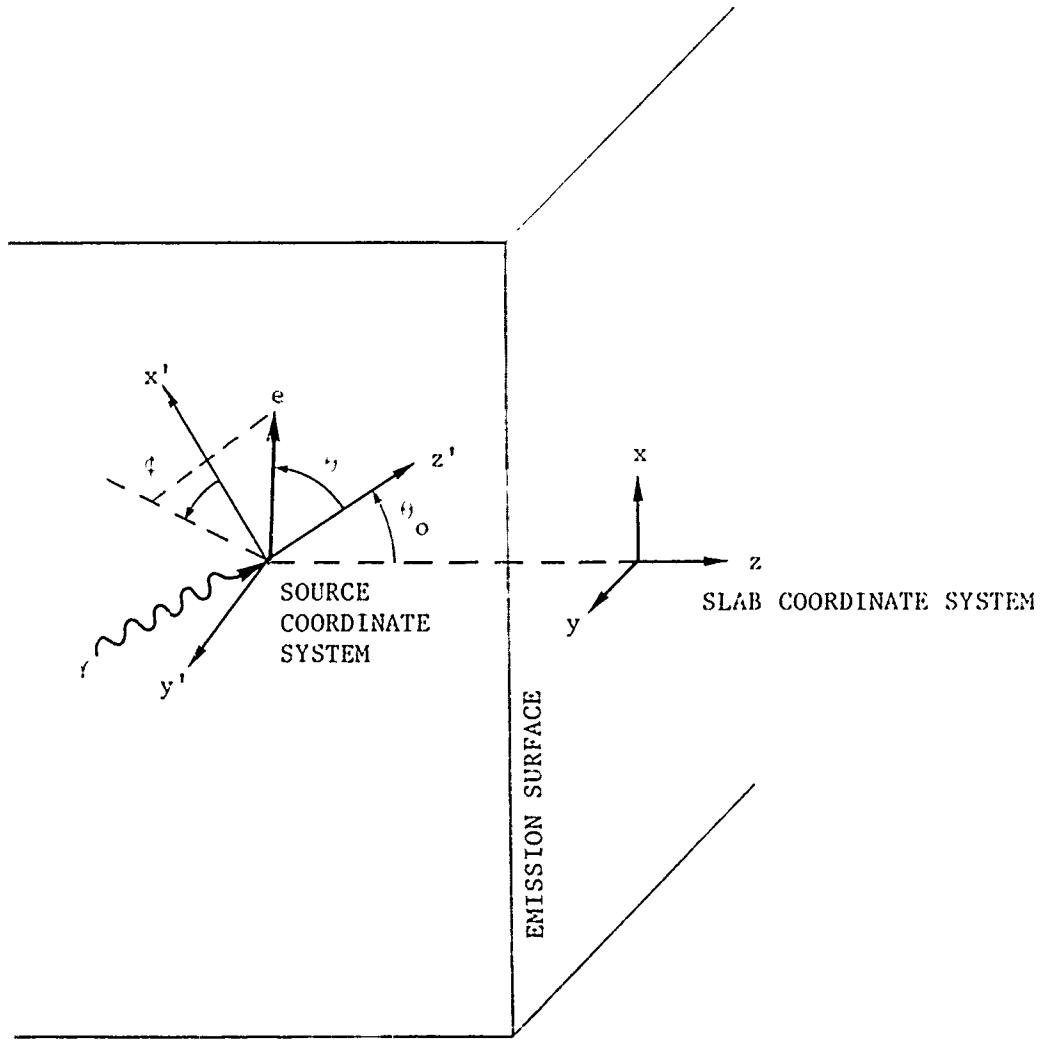

Figure 9

COORDINATE SYSTEM x'y'z' FOR ELECTRON SOURCE

The electron source density S and the energy-angular distribution $H(E_i,\theta_j)$ define the electron source for input to the electron transport calculation.

3.2 ELECTRON TRANSPORT

POEM calculates the electron transport using the Monte Carlo method. The transport is simulated by tracing the trajectories of many particles through a random walk calculation. The initial conditions for each particle - energy, direction, and location - are random selected from the electron source probability distributions. The weight of each particle is determined by the electron source density. The trajectory of the particle is traced using precalculated slowing down and scattering distributions. Relevant quantities - energy and charge currents at zone boundaries and energy and charge depositions within zones - are scored for each trajectory. Estimates of the desired output quantities and estimates of the statistical errors are made by averaging the results for many particle histories.

3.2.1 The Monte Carlo Method

As an example of the Monte Carlo method used in POEM, we discuss the calculation of the electron emission from a planar surface. Extension of the method to the transition zone dose and current calculation is straightforward. We express the yield in electrons/photon-Sr-keV as a function $y'(E_i,\theta_j,\phi_k)$ over a three-dimensional array of n_i energy bins, n_j θ-angle bins, and n_k ϕ-angle bins. Each bin is characterized by its midpoint, for example, the energy bin E_i contains the energy interval $(E_i - \Delta E/2, E_i + \Delta E/2)$. Let N_e (electrons/cm^2) be the density of electrons produced in the source region. Let $F(E,\theta,\phi,z)$

be the cumulative probability distribution function for the initial energy E, direction (θ,ϕ), and location z of the electrons. The yield is then given by

$$y'(E_i,\theta_j,\phi_k) = N_e \int p(E_i,\theta_j,\phi_k|E,\theta,\phi,z)$$

$$dF(E,\theta,\phi,z) \qquad (27)$$

where $p(E_i,\theta_j,\phi_k|E,\theta,\phi,z)$ is the probability that an electron with initial energy E, direction (θ,ϕ), and location z is emitted into energy bin E_i, θ-angle bin θ_j, and ϕ-angle bin ϕ_k. Let the vector $\underline{X} = (E,\theta,\phi,z)$ define the initial electron conditions. We denote $y_{ijk} = y'(E_i,\theta_j,\phi_k)$ and $p_{ijk}(\underline{X}) = p(E_i,\theta_j,\phi_k|E,\theta,\phi,z)$. The equation can be rewritten as

$$y_{ijk} = N_e \int p_{ijk}(\underline{X})\, dF(\underline{X}). \qquad (28)$$

POEM uses the Monte Carlo method to evaluate the integral in Equation (28). Particles are started with initial conditions selected from the source distribution $F(\underline{X})$, and the particle trajectories are traced until the particle is emitted from the surface, or until the residual range of the particle is insufficient for the particle to reach the surface. For particle number n we define the random variable $\xi_{ijk}(n)$ by

$$\xi_{ijk}(n) = \begin{cases} 1, \text{ if particle n is emitted with conditions } E_i,\theta_j,\phi_k \\ 0, \text{ otherwise} \end{cases} \qquad (29)$$

We define the random variable $Y_{ijk}(N)$ as

$$Y_{ijk}(N) = \frac{N_e}{N} \sum_{n=1}^{N} \xi_{ijk}(n). \tag{30}$$

We calculate $Y_{ijk}(N)$ by tracing the trajectories of N particles. Each time a particle is emitted with conditions (E_i, θ_j, ϕ_k), we increment $Y_{ijk}(N)$ by N_e/N. The expected value of $Y_{ijk}(N)$ is y_{ijk}:

$$E\left\{Y_{ijk}(N)\right\} = \frac{N_e}{N} \sum_{n=1}^{N} E\left\{\xi_{ijk}(n)\right\}$$

$$= \frac{N_e}{N}\left[N \int p_{ijk}(\underline{X})\, dF\,(\underline{X}) \right] = y_{ijk} \tag{31}$$

The calculated quantity $Y_{ijk}(N)$ is called an unbiased estimator of the yield y_{ijk}. The law of large numbers tells us that for any $\varepsilon > 0$,

$$\lim_{N \to \infty} \text{prob}\left\{ |Y_{ijk}(N) - y_{ijk}| \leq \varepsilon \right\} = 1 \tag{32}$$

That is, $Y_{ijk}(N)$ tends to y_{ijk} in probability. Thus, if we calculate a sufficient number of particle histories, we can estimate the yield y_{ijk} by the estimator $Y_{ijk}(N)$ to to within arbitrary precision.

The variance of the estimator $Y_{ijk}(N)$ is

$$\text{VAR}\left\{Y_{ijk}(N)\right\} = E\left\{(Y_{ijk}(N) - y_{ijk})^2\right\} = \frac{1}{N}\,\sigma_p^2 \tag{33}$$

where

$$\sigma_p^2 = \int [p_{ijk}(\underline{X}) - y_{ijk}]^2 dF(\underline{X}) \tag{34}$$

is the variance of the emission probability distribution $p_{ijk}(\underline{X})$. The square root of the variance of $Y_{ijk}(N)$ is the standard error

$$\sigma_Y(N) = \frac{1}{\sqrt{N}} \sigma_p. \tag{35}$$

Equation (35) shows that the statistical error $\sigma_Y(N)$ is inversely proportional to the square root of the number of particle histories. Thus, to reduce the error by a factor k requires increasing the number of particle histories by a factor of k^2.

The standard error σ_Y is not a computed quantity in the Monte Carlo calculation. However, just as we obtain an estimator for the yield y_{ijk} we obtain an estimator for the standard error. The unbiased estimator for σ_Y is s where s^2 is given by

$$s^2 = \frac{1}{N-1} \left[\frac{1}{N} \sum_{n=1}^{N} g^2(\underline{X}_n) - Y_{ijk}^2(N) \right]. \tag{36}$$

3.2.2 Variance Reduction

Using the Monte Carlo method we can obtain predictions for the yield $y'(E_i, \theta_j, \phi_k)$ and the statistical error of the estimated yield. The problem is that emission of a particle into any one of the bins (E_i, θ_j, ϕ_k) of the three-dimensional emission distribution is an infrequent event. For example, for back emission from aluminum irradiated by

10 keV x-rays, the mean probability of emission of a source region electron is 0.058. The mean probability for the emission of the electron into one of 20 bins of a one-dimensional angular distribution is 0.0029. The mean probability for emission into one of the 160 bins of a two-dimensional angular distribution over 20 θ-bins by 8 ϕ-bins is 0.00036. This means that in a straightforward Monte Carlo calculation one would expect on the average four particles out of 10,000 histories to be emitted into any one bin of the two-dimensional angular distribution. To obtain a statistically meaningful distribution would require many hundred-thousand histories at considerable computation expense.

Since to halve the standard error one must quadruple the number of particle histories, error reduction through increased numbers of particle histories is inefficient. A more efficient method of error reduction is to reduce the standard deviation σ_p of the parent distribution rather than increase the number of histories N [Equation (35)]. This can be done through variance reduction techniques.

Variance reduction in Monte Carlo can be viewed as the introduction of known, usually qualitative, information about the process being simulated into the Monte Carlo simulation in an explicit and quantitative manner. Through the introduction of such information, the amount of information which must be obtained through the simulation is reduced. Variance reduction techniques for radiation transport calculations are highly developed - through judicious application of these techniques code efficiencies can in some cases be increased by factors of up to several thousand. A good mathematical treatment of variance reduction is found in Reference 17; a convenient, practical discussion is found in Reference 18.

The variance reduction technique which has been used to most advantage in POEM is importance sampling. The electrons which contribute most significantly to the emission are sampled preferentially through biasing the electron source distributions. The weights of the transport particles are adjusted accordingly so as not to bias the estimator. Importance sampling increases the number of particle emissions and decreases the computation time wasted on those particles which do not contribute to the emission distribution. Through importance sampling the POEM code efficiency has been increased by about a factor of 20; i.e., to obtain the same standard error the code with importance sampling requires 1/20 the computation time required for straightforward Monte Carlo.

To illustrate the importance sampling concept, consider a one-dimensional simplification of the integral in Equation (28):

$$y = N_e \int p(x)\ dF(x). \tag{37}$$

Where y is yield, p(x) is the probability of emission given initial condition x and F(x) is the cumulative probability distribution for x. Rather than compute this integral, we compute the integral

$$y = N_e \int \frac{p(x)}{g(x)}\ dF'(x) \tag{38}$$

where

$$dF'(x) = g(x)dF(x) = g(x)f(x)dx \tag{39}$$

We track N particles selecting their initial condition x_n from the cumulative probability distribution function F' rather than F and weight the particles by $1/g(x_n)$. Just as before we define an estimator Y'(N):

$$Y'(N) = \frac{N_e}{N} \sum_{n=1}^{N} W_n \xi_n \tag{40}$$

where

$$\xi_n = \begin{cases} 1, \text{ if particle n is emitted} \\ 0, \text{ otherwise} \end{cases} \tag{41}$$

and

$$W_n = \frac{1}{g(x_n)}$$

The expected value of the estimator is

$$E\{Y'(N)\} = \frac{N_e}{N} \sum_{n=1}^{N} E\{W_n \xi_n\}$$

$$= \frac{N_e}{N} \left[N \int \frac{p(x)}{g(x)} \, dF'(x) \right] = y \tag{42}$$

Thus, Y'(N) is an unbiased estimator of y. The standard error $\sigma_{Y'}$ is

$$\sigma_{Y'} = \frac{1}{\sqrt{N}} \sigma_{p/g} \tag{43}$$

where $\sigma_{p/g}$ is the standard deviation of distribution $p(x)/g(x)$. If $g(x)$ is a reasonable approximation of $p(x)$ over the range of x, i.e., $g(x) \approx p(x)$, $x_{min} \leq x \leq x_{max}$, then the standard deviation $\sigma_{p/g}$ will be small compared with the standard deviation σ_p of the distribution $p(x)$. Therefore, comparing Equations (35) and (43), the standard error σ_Y, for the calculation using importance sampling will be small compared with the standard error σ_Y for the calculation using the straightforward Monte Carlo.

To incorporate importance sampling into the emission calculation we bias the sampling distribution $f(x)$ for the electron initial conditions with a function $g(x)$ which is the best approximation obtainable of the probability of emission $p(x)$. In POEM importance sampling is used in the selection of the particle initial location and initial energy.

For electrons of initial energy E and range R(E), emission is possible only for those electrons with initial location at distance from the surface $z < R(E)$. Thus, in POEM, initial location is sampled only over the range $0 \leq z < R(E)$. The particles are weighted by $W = R(E)\Delta z$ where Δz is the thickness of the source region. Because of scattering, electrons with a given range R(E) which start nearer the surface have higher probability of emission. In POEM, the sampling distribution for initial electron distance z from the surface is biased by a linear function $g(z)$ which is zero at $z = R(E)$ and maximum at $z = 0$. The particle weight is multiplied by a factor $1/g(z)$.

Within the source region, electrons with higher initial energy have higher probability of emission. In POEM, the sampling distribution for initial electron energy is biased towards high energy. The biasing and weighting are performed in the random selection procedure as explained in Section 3.2.4.

Importance sampling is not used in POEM for the selection of initial electron direction. Clearly importance sampling could be advantageous here - those electrons starting in a direction towards the surface have higher probability of emission than those starting in a direction away from the surface. Appropriate biasing of the sampling distribution for initial direction is currently being investigated.

Another form of importance sampling used in POEM is particle killing. A particle whose residual range is less than the minimum distance to an emission surface (or deposition zone boundary) is killed since it cannot contribute to the distribution. This is an obvious variance reduction technique which is also available in such codes as ETRAN and SANDYL.

Other variance reduction techniques are being tried in experimental versions of POEM. These include track splitting, control variates, and orthonormal polynomial expansions of output distributions. These techniques, if proven effective, will be incorporated into POEM and reported in subsequent publications.

3.2.3 Transport Grid

POEM is a multiple-scatter electron transport code. Rather than directly simulate each collision, as is commonly done in photon transport codes, each step of the random walk calculation simulates the effects of many collisions. The step sizes, the energy loss increments, and the multiple scattering probability distributions corresponding to each step of the random walk are predetermined using the code DATAGEN.

An energy grid is set up using logarithmic energy steps from the maximum electron energy down to 1 keV. Typically, the energy step sizes are set such that an electron loses one-half of its energy in eight steps. The number of steps to halve the energy is NCYC. The energy of each successive grid point is reduced by a factor EFAC where EFAC**NCYC = 1/2:

$$E(N) = E(N-1) * EFAC. \tag{44}$$

At low energies, E≤10 keV, it is found that the energy steps are needlessly small for NCYC = 8, particularly for high-Z materials. The corresponding spatial step sizes are so small that there is a sizable probability of zero deflection along the step. Consequently, the logarithmic spacing of the energy grid is modified below about 10 keV. Typically we set NCYC = 8 at high energies, change to 4 at about 10 keV, and to 2 at about 5 keV.

To insure sufficient detail in the random walk calculation, the major energy grid is subdivided into NSUB substeps:

$$\Delta E(N) = \frac{E(N) - E(N+1)}{NSUB} \tag{45}$$

The appropriate value for NSUB depends on the transport medium atomic number, and also to some extent on the user application. Higher atomic number materials require more substeps. We have obtained good results for NSUB values typified by Table 5. (These values are somewhat smaller than those given by the empirical formula recommended for SANDYL.[2])

Table 5

TYPICAL NSUB VALUES

MATERIAL	Z	NSUB
C	6	2
Al	13	4
Sn	50	6
Au	79	8

POEM uses the continuous slowing down (csda) approximation: the spatial step size Δs is uniquely determined by the energy step size ΔE. (POEM neglects energy loss straggling. This does not appear, however, to be an important effect in the x-ray photoemission or transition zone dose applications for which POEM was designed - we obtain good agreement with experiment. Thus, the inclusion of straggling does not at this time appear to warrant the cost, i.e., the attendant degradation of code efficiency.) The spatial step size Δs is calculated from the slowing down distribution $dE/ds(E)$:

$$\Delta s = \int_{E}^{E-\Delta E} \frac{dE}{-dE/ds} \, . \tag{46}$$

The stopping power $-dE/ds$ includes both collision and radiation terms

$$\frac{dE}{ds} = \left(\frac{dE}{ds}\right)_{col} + \left(\frac{dE}{ds}\right)_{rad} . \tag{47}$$

In traversing the pathlength increment Δs, the electron undergoes a number of single scatterings. The probability distribution for the total deflection of the electron is calculated using the Goudsmitt-Saunderson multiple scattering theory. One distribution is calculated for each point N of the major energy grid. A cumulative probability distribution $G_N(\theta)$ is calculated for an electron of energy E_N for energy loss ΔE and pathlength increment Δs. The distribution is calculated over an angular grid defined by the endpoints θ = 0.5, 1.0, 1.5, 2, 3, 4, 6, 8, 10, 15, 20, 30, 40, 60, 80, 100, 120, 140, 160, and 180 degrees.

The transport grid - the major energy grid endpoints E_N, the energy substeps ΔE_N, the pathlength increments Δs_N, and the multiple scattering distributions $G_N(\theta)$ are calculated by the code DATAGEN and are stored for use in the random walk calculation.

3.2.4 Random Walk

The random walk calculation for each particle starts with random selection of the initial energy, direction, and location and proceeds through spatial steps and angular deflections until the particle escapes the transport region or is absorbed. Along the particle trajectory, zone and material boundary crossings are scored. In the following paragraphs, we discuss the procedures for trajectory origination, trajectory construction, trajectory termination, boundary crossings, and scoring.

Trajectory Origination - The electron history starts with random selection of the initial energy E_o. The cumulative distribution function $F_E(E)$ is determined from the cumulative, two-dimensional source distribution $H(E,\theta)$ [Equation (26)]:

$$F_E(E) = H(E,\pi). \tag{48}$$

The energy E_o is selected by generating a random number r_o between 0 and 1 and setting $E_o = F_E^{-1}(r_o)$ where F_E^{-1} is the inverse of the distribution function F_E. The procedure is illustrated in Figure 10. If r_o were selected from the uniform distribution over the interval 0 to 1, U(0,1), then the selected distribution of initial energies would simulate the source distribution; i.e., after many histories, the selected initial energy cumulative distribution would approach $F_E(E)$. We, however, want to bias the sampling distribution towards high energy. We select a random number u_o from U(0,1) and then set $r_o = 1 - u_o^2$. This bias was found by experience to maximize the code efficiency over the range of application. The appropriate particle weight factor can be shown to be

$$W_E = 2u_o. \tag{49}$$

Note that the initial energy is not selected from a discrete distribution but from a continuous distribution. This is done by linear interpolation in the stored, discrete source distribution, as is indicated graphically in Figure 10.

Next, the initial distance z_o from the surface is selected. The source density is assumed uniform over the source region, $0 \leq z_o \leq \Delta z$. The electron of initial energy E_o can only be emitted, however, from the region $0 \leq z_o \leq R(E_o)$. Thus, the sampling is restricted to the region $0 \leq z_o \leq R(E_o)$. Accordingly, the particle weight is modified by the factor $R(E_o)/\Delta z$. We want to bias the sampling distribution towards $z_o = 0$. A linear sampling distribution is used which is maximum at $z_o = 0$ and zero at $z_o = R(E)$. This is effected

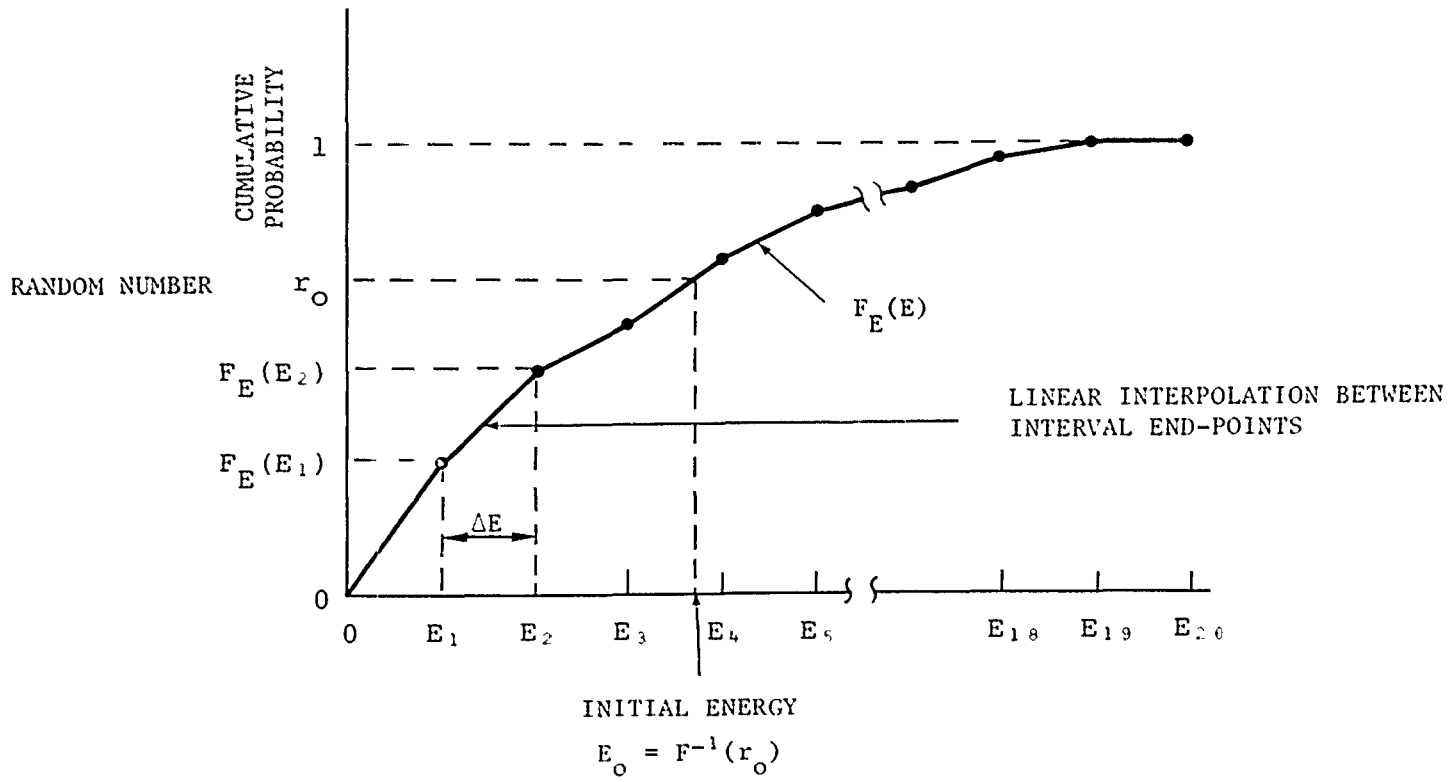

Figure 10

RANDOM SELECTION OF INITIAL ENERGY
FROM CUMULATIVE PROBABILITY DISTRIBUTION

by selecting a random number u_o from U(0,1), setting $r_o = \sqrt{u_o}$, and setting

$$z_o = (1 - r_o)R(E_o). \tag{49}$$

The appropriate weighting factor is $1/2r_o$. The total weighting factor W_z for the z selection is then

$$W_z = \frac{1}{2r_o} \frac{R(E_o)}{\Delta z} . \tag{50}$$

Selection of the initial energy E_o determines the distribution function for the initial θ-angle. Let the selected initial energy E_o be in the energy group E_N of the cumulative source distribution function $H(E,\theta)$. The cumulative distribution function F_θ for the initial θ-angle (with respect to the photon direction of incidence) is

$$F_\theta(\theta) = \frac{H(E_N,\theta) - H(E_N,0)}{H(E_N,\pi) - H(E_N,0)} . \tag{51}$$

No biasing is used in the selection of the angle θ_o. A random number u_o is selected from U(0,1). The initial angle θ_o', with respect to the photon direction of incidence, is selected using the same procedure as for the selection of the initial energy E_o:

$$\theta_o' = F_\theta^{-1}(u_o) \tag{52}$$

θ_o' just as E_c, is selected from a continuous distribution through linear interpolation in the computed, discrete source distribution.

An initial azimuthal angle ϕ_o' is selected from a uniform distribution about the photon direction of incidence. A random number u_o is selected from U(0,1), and ϕ_o' is set

$$\phi_o' = u_o \cdot 2\pi \ . \tag{53}$$

The initial direction (θ_o', ϕ_o') is selected from angular distributions defined with respect to the photon direction of incidence. Transformation to the direction (θ_o, ϕ_o) in the problem geometry coordinate system is performed using a straightforward orthogonal transformation.

The total weight W_o of the particle is the product of the weight factors W_E and W_z,

$$W_o = W_E W_z \ . \tag{54}$$

Trajectory Construction - A particle of weight W_o and initial energy E_o starts out at location z_o and direction (θ_o, ϕ_o). The particle takes a partial step to reduce its energy to the nearest lower point of the transport energy grid. Let the initial energy E_o be bound by the major energy grid points E_N and E_{N+1}, $E_N \geq E_o > E_{N+1}$, and let δE be the energy loss increment required to reach the next subdivision point of the energy grid. Then the partial step size δs is calculated by linear interpolation:

$$\delta s = \frac{\delta E}{\Delta E_N} \ \Delta s_N \ . \tag{55}$$

Thereafter, the calculation steps through the transport grid, incrementing the pathlength and decreasing the

particle energy. At the end of each pathlength increment Δs_N, the code samples the angular deflection $\Delta\theta_N$, with respect to the present direction of travel, from the multiple scattering distribution $G_N(\theta)$. The angle is calculated by selecting a random number u_o from U(0,1) and setting

$$\Delta\theta_N = G_N^{-1}(u_o) \quad . \tag{56}$$

The angular deflection is sampled from a continuous distribution through linear interpolation in the stored discrete distribution G_N. The azimuthal deflection $\Delta\theta_N$ is selected from a uniform distribution $(0,2\pi)$ about the present direction of travel. The new direction of travel (θ,ϕ) at the end of the pathlength increment is found using $\Delta\theta_N$, $\Delta\phi_N$, and the old direction (θ',ϕ') in an orthogonal transformation.

After each step, the new particle position z is calculated:

$$z = z' + \Delta s_N \cos\theta_N \tag{57}$$

where z' is the former position. The distance $|z - z_{BND}|$ to the nearest boundary is calculated. (For the emission calculation, this boundary is the emitting surface.) If this direction is greater than the particle residual range $R(E_N)$, then the trajectory is terminated.

If the particle has crossed a boundary during a step, then the energy of the particle at the boundary is found by linear interpolation. If E_N is the energy at the start of the step, and δs is the distance along the particle path from the start of the step to the intersection of the path with the boundary, then the energy of the particle at the boundary is

$$E_{BND} = E_N - \frac{\delta s}{\Delta s_N} \Delta E_N \quad . \tag{58}$$

The charge current at the boundary is incremented by the particle weight W. The energy current is incremented by $W \cdot E_{BND}$. If the boundary is the emission surface, the particle weight W is scored in each of the appropriate energy, θ-angle and ϕ-angle bins of the emission distribution.

If the boundary crossed by the particle is an interface between different materials, the particle is backed up to the point of intersection of the path with the boundary. The particle then starts into the new material with energy E_{BND} and the same direction of travel as when it reached the boundary. The first step in the new material is a partial step, following the same partial step procedure as at the start of the trajectory.

The particle trajectory is terminated with the residual range is less than the distance to the nearest boundary, or when the energy has decreased to 1 keV. A new trajectory is then started. This process is continued until the desired number of particle histories has been calculated. In order to preclude the disaster of exceeding the CP time limit before obtaining results, POEM checks on CP time during the random walk calculation. If the time limit is approached, POEM will terminate the random walk calculation and move on to the calculation of the results.

3.3 TRANSITION ZONE DOSE AND CURRENT PROFILES

Extension of the above electron source and transport computational procedures to the calculation of the dose and current profiles near a material interface could be straight-

forward: calculate the source densities and distributions on both sides of the interface, and calculate the transport in the neighborhood of the interface. We, however, have found it advantageous to be somewhat devious. In the straightforward approach we would spend considerable time tracking particles in the transition zone whose trajectories never cross the interface. The trajectories of these particles are independent of the nature of the material on the opposite side of the interface. In particular, their trajectories would be the same if the transport region were in electron equilibrium (i.e., the region were in an unbounded medium). We know the equilibrium dose and current (the kerma and the PC current in an unbounded medium). These are readily obtainable from tabulations or by analytical codes.[19 20] When available, analytical methods are always preferable to Monte Carlo methods. By restricting the Monte Carlo calculation to the nonequilibrium contributions to the dose and current, considerable reduction in variance is achieved. Furthermore, it increases physical insight into processes determining the characteristics of the dose and current profiles.

Consider a planar interface between two materials, A and B. We wish to calculate the photo-Compton (PC) current and the dose distribution in B near the interface. Let J_A be the PC current in B of electrons arising in A, and let $J_{B/A}$ be the PC current of electrons arising in B which have been backscattered from A. Now consider the interface when the slab A is replaced by a slab B' of composition identical to material B. (The interface is now a plane in the midst of an unbounded region of material B.) Let $J_{B'}$ be the PC current in B of electrons arising in B' and $J_{B/B'}$ be the PC current in B of electrons arising in B which have been backscattered from B'. Finally, let

J_{EQ} be the equilibrium PC current in B (the PC yield in an unbounded region of B). Then the total PC current in B near the interface with A is given by

$$J(z) = J_{EQ} + [J_A(z) - J_{B'}(z)] + [J_{B/A}(z) - J_{B/B'}(z)]. \quad (59)$$

The first bracketed term in Equation (59) represents the nonequilibrium component of the PC current due to emission from the interfacing material. The second bracketed term represents the nonequilibrium component due to backscatter from the interfacing material. A similar expression can be obtained for the dose:

$$D(z) = D_{EQ} + [D_A(z) - (D_{B'}(z)] + [D_{B/A}(z) - D_{B/B'}(z)] \quad (60)$$

where D_{EQ} is the kerma.

Monte Carlo calculations are performed to obtain each of the nonequilibrium terms for the PC current - J_A, $J_{B'}$, $J_{B/A}$, and $J_{B/B'}$ in Equation (59) -- and the corresponding PC vector energy currents. The nonequilibrium terms for the dose - D_A, $D_{B'}$, $D_{B/A}$, and $D_{B/B'}$ in Equation (60) - are obtained by differentiating the electron energy currents. The equilibrium PC current can be obtained from the Dellin and MacCallum handbook.[20] The kerma can be obtained from standard tables.[19]

The relative magnitudes of the terms in Equations (59) and (60) vary with photon energy. For example, for

dose in a low-Z material near a high-Z material, $D_A(x)$ is very large compared with any of the other terms for photon energies less than about 100 keV. But for photons with energies greater than about 1000 keV, incident through the low-Z material, the term $D_{B/A}(x)$ dominates. For maximum efficiency, the number of particle histories allocated to the calculation of each of the terms should be directly proportional to its relative contribution to the sum. It is planned to automate this allocation procedure. In the meanwhile, some user intuition is required, perhaps aided by the forthcoming report on transition zone dose and current.

POEM also calculates analytic functional fits to the Monte Carlo calculated dose and current profiles. The interest in fits is twofold. First, analytic expressions are of course more convenient for representing results than are tabulations of Monte Carlo data. Second, it is hoped to "damp out" statistical fluctuations in the charge and energy current profiles. The Monte Carlo predictions of the charge deposition and dose are obtained through first-order finite differencing of the charge and energy currents. For deposition zone number n,

$$Q_n = \frac{j(z_{n-1}) - j(z_n)}{\Delta z} \tag{61}$$

$$D_n = \frac{f(z_{n-1}) - f(z_n)}{\rho \Delta z} \tag{62}$$

where $j(z_n)$ and $f(z_n)$ are the charge and energy currents, respectively, at zone boundary z_n. This is the crudest form of numerical differentiation. Even if the statistical errors for j and f are small, the errors for Q and D will be large

if Δz is small. If one could accurately represent $j(z)$ and $f(z)$ with analytic expressions, then the differentiation could be performed analytically.

POEM fits the Monte Carlo calculated charge and energy current profiles to expressions of the form

$$f(z) = A \exp(Bz + Cz^2 + Dz^3). \tag{63}$$

Fits to the deposition profiles are obtained through analytical differentiation of the expression in Equation (63):

$$\frac{df(z)}{dz} = (B + 2Cz + 3Dz^2)\ f\ (z) \tag{64}$$

Representative fits to the charge current profile and to the energy deposition profile are shown in Figure 11. The fits to the current profiles are consistently quite good. The fits to the deposition profiles, however, are not uniformly satisfying, for example as shown in Figure 12. The reason for the discrepancy is that for the contribution due to electron emission from the high-Z material - the $D_A(z)$ term - the various source electron groups - Compton, K-photo, L-photo, and Auger - produce characteristically different energy deposition profiles in the low-Z material. The fit can be considerably improved by separately calculating and fitting the profiles for each of the source groups, and then summing the contributions (Figure 13). The POEM code has this capability, which may be exercised as an option.

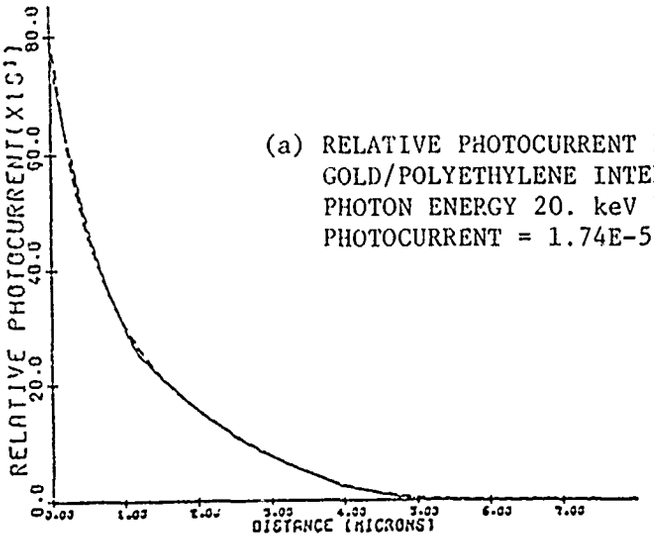

(a) RELATIVE PHOTOCURRENT PROFILE
GOLD/POLYETHYLENE INTERFACE
PHOTON ENERGY 20. keV EQUILIBIUM
PHOTOCURRENT = 1.74E-5 ELEC/PHOT

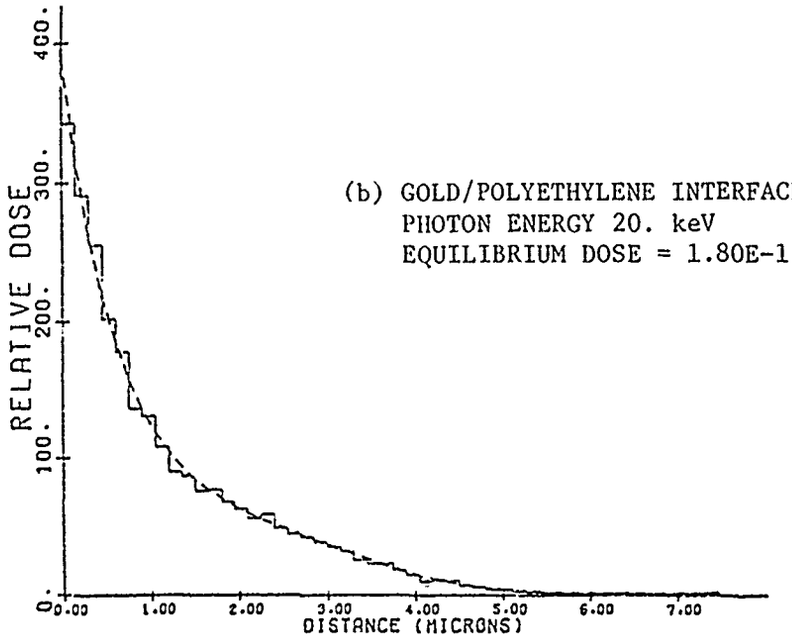

(b) GOLD/POLYETHYLENE INTERFACE
PHOTON ENERGY 20. keV
EQUILIBRIUM DOSE = 1.80E-1 gm/cm^2

Figure 11

RELATIVE DOSE PROFILE

(Plots courtesy of J.C. Garth, Air Force Cambridge Research Laboratories)

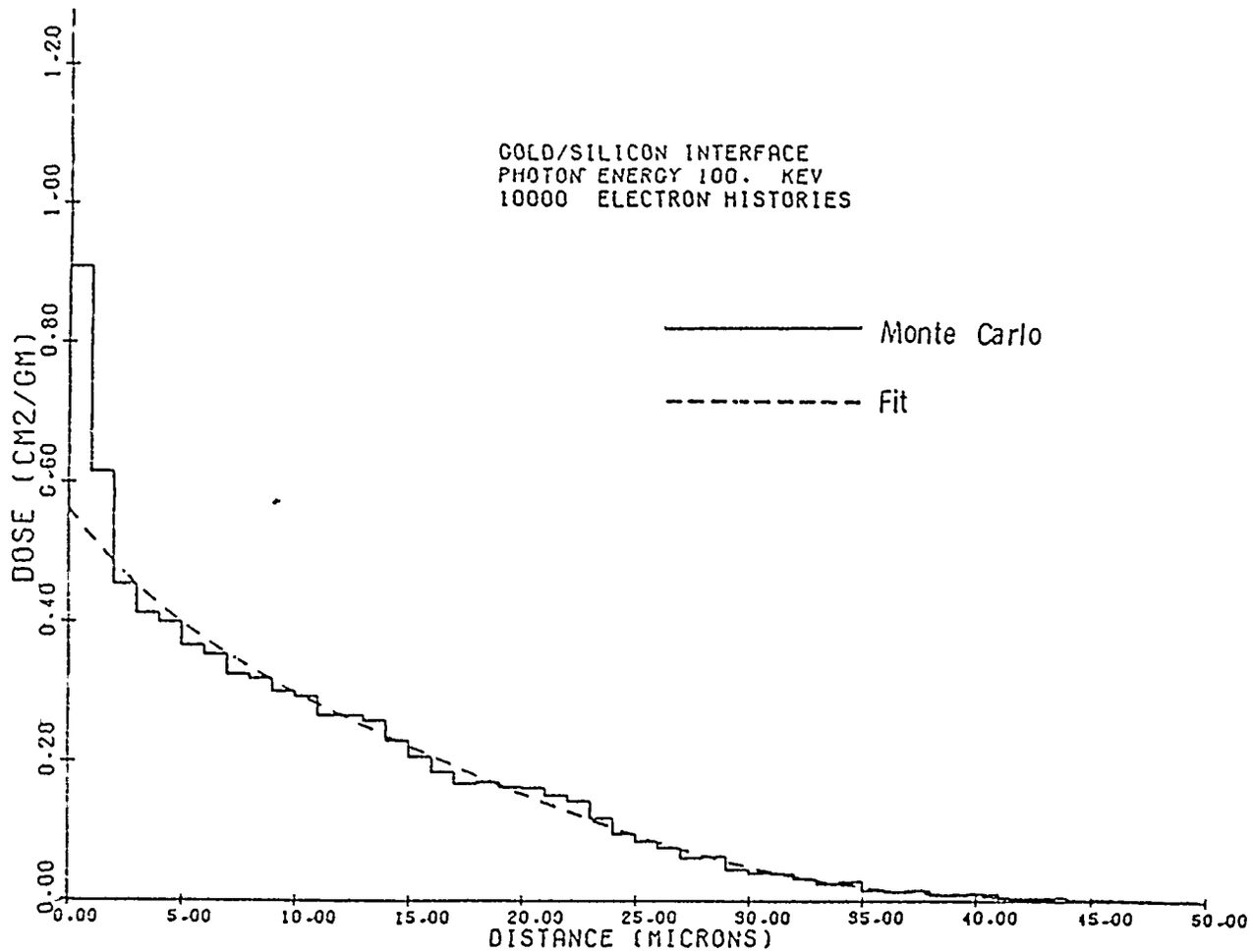

Figure 12

ENERGY DEPOSITION PROFILE IN SILICON

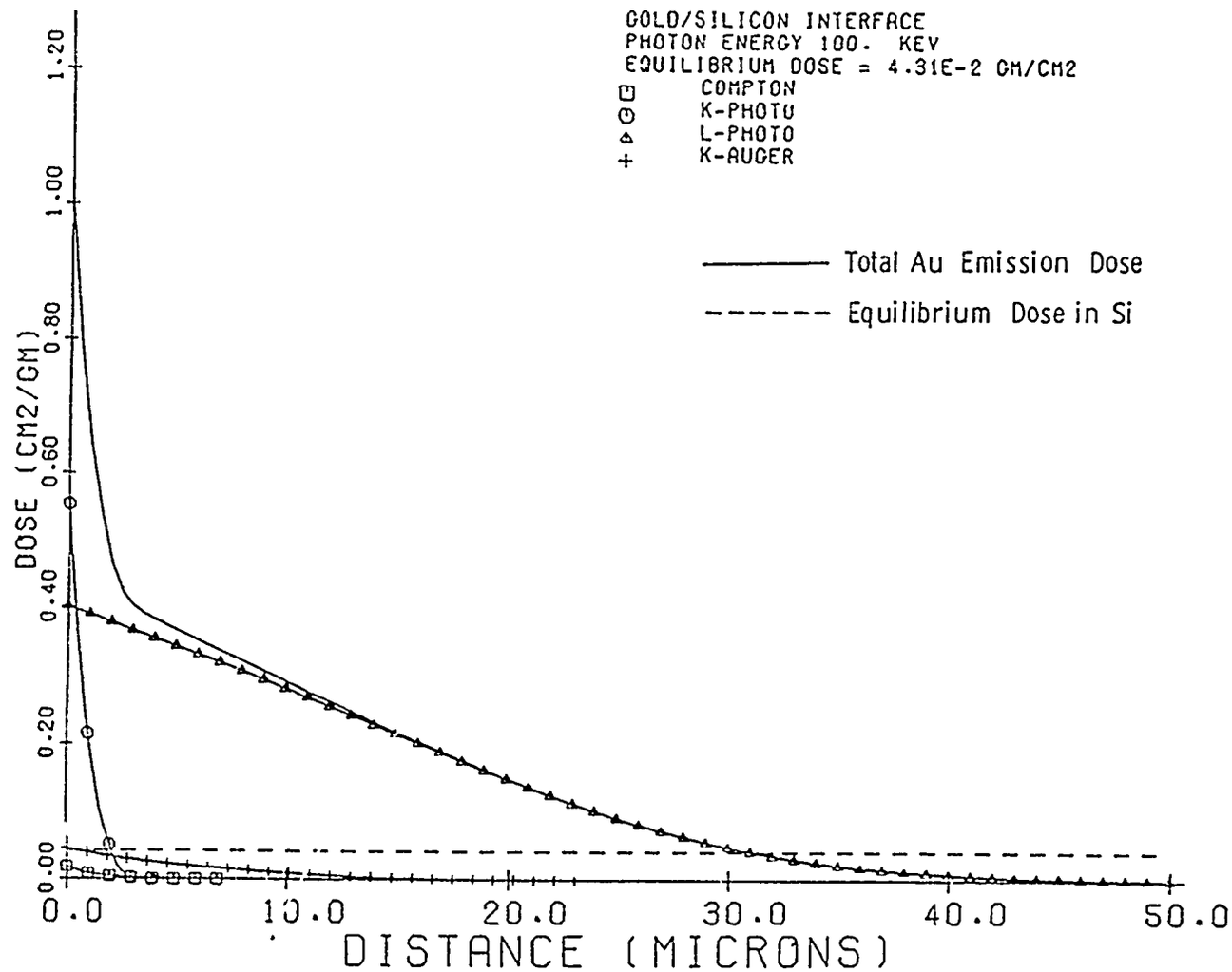

Figure 13
ABSOLUTE DOSE PROFILE

Section 4

CROSS SECTIONS

4.1 ELECTRON PRODUCTION

Three electron production mechanisms are included in POEM: the Compton, photoelectric, and Auger effects. Pair production and secondary electron production are not included.

4.1.1 Compton Electrons

The density and energy-angular probability distribution of the Compton electrons are calculated using the theory of Klein and Nishina. The mathematical expression for the total interaction cross section is taken from Evans:[21]

$$\sigma\left(\frac{cm^2}{g}\right) = \frac{N_o Z}{A} \; 2\pi r_o^2 \left\{ \frac{1+\alpha}{\alpha^2} \left[\frac{2(1+\alpha)}{1+2\alpha} - \frac{1}{\alpha} \ln(1+2\alpha) \right] + \frac{1}{2\alpha} \ln(1+2\alpha) - \frac{1+3\alpha}{(1+2\alpha)^2} \right\} \qquad (65)$$

where $\alpha = h\nu/mc^2$ and $r_o = e^2/mc^2$. The expression for the energy distribution is taken from Evans:[30]

$$\frac{dp(E)}{dE} = A \left\{ 2 + \left(\frac{E}{h\nu - E} \right)^2 \cdot \left[\frac{1}{\alpha^2} + \frac{h\nu - E}{h\nu} - \frac{2}{\alpha} \frac{h\nu - E}{E} \right] \right\} \qquad (66)$$

where A is a constant.

Once the electron energy E is determined, the scattering angle θ of the electron is found from the relativistic expressions for conservation of energy and momentum:

$$\tan\theta = \frac{1}{1+\alpha} \sqrt{2\alpha\left(\frac{h\nu}{E} - 1\right) - 1} \tag{67}$$

4.1.2 Photoelectrons

The total photoelectric cross section is found using log-log interpolation with the ENDF/B[23] photon cross section compilation. We have extracted the photoelectric cross sections from the ENDF/B compilation for the elements Z = 1 through 83, 86, 90, 92, and 94 and stored the cross sections on the photon interaction data tape. The tape also contains the relative shell ionization probabilities and the K, mean L and mean M absorbtion edges as discussed in Section 3. The mean N edge is approximated by zero.

The angular distribution of the photoelectrons is calculated using the Fischer[22] formula for low energy electrons, $E \leq E_c$:

$$\frac{dp(\theta)}{d\theta} = A \frac{\sin^3\theta}{(1-\beta'\cos\theta)^4} \tag{68}$$

$$\beta' = \frac{\beta}{1+h\nu/2mc^2} \tag{69}$$

and the Sauter formula for high energy electrons, $E > E_c$:

$$\frac{dp(\theta)}{d\theta} = A' \frac{\sin^3\theta(1 + \beta''\cos\theta)}{(1 - \beta\cos\theta)^4} \tag{70}$$

$$\beta'' = \frac{\beta}{\frac{2}{T(1+T^2)} - 1}, \quad T = E/mc^2 \tag{71}$$

where the transition electron energy E_o is that recommended by Dellin and MacCallum:[24]

$$E_o = 2.5Z - 0.5E_K \tag{72}$$

4.1.3 Auger Electrons

The K and mean L fluorescence yields have been obtained from the compilation of Bambynek, et al.[25] and from the fitted data of Storm and Israel,[19] where not available from the Bambynek compilation, and stored on the photon interaction data tape. The mean M fluorescence yield is approximated by zero. The angular distribution of the Auger electrons is isotropic.

4.2 ELECTRON TRANSPORT

4.2.1 Energy Loss

POEM uses the continuous slowing down approximation. Energy loss ΔE is uniquely determined by pathlength increment Δs. The energy loss $-dE/ds$ includes two terms, collision and radiation:

$$\frac{dE}{ds} = \left(\frac{dE}{ds}\right)_{col} + \left(\frac{dE}{ds}\right)_{rad} . \tag{73}$$

The collision term is calculated using the expressions of Berger and Seltzer[26] for the Rohrlich and Carlson formulation of the Bethe stopping power theory with the Sternheimer density effect correction. For $Z \geq 13$, the empirical relation of Sternheimer[26] is used for the mean excitation energy. For $Z < 13$, the tabulated values of Reference 26 are used.

For the POEM code range of application, the radiation loss term is small compared with the collision loss term. A simple, approximate formulation of the radiation loss term has proven adequate. The collision loss is calculated as

$$\left(-\frac{dE}{ds}\right)_{rad} = NE\,\bar{\Phi}\,(Z)R(E,Z) \tag{74}$$

where N is the density (atoms/cm), E is the electron energy, $\bar{\Phi}$ is given by

$$\bar{\Phi} = \frac{Z(Z+1)}{137}\,r_o^2 \tag{75}$$

where $r_o = e^2/mc^2$. R is given by a least-squares fit to the data of Berger and Seltzer:[26] for E<1 MeV, R is constant; for 1 MeV$\leq$E$\leq$10 MeV, log R is a linear function of log E.

4.2.2 Scattering

The probability distribution $G_N(\theta)$ for the angle θ through which the electron is scattered in traversing a pathlength increment Δs_N is calculated using the multiple scattering theory of Goudsmitt and Saunderson as implemented by Berger in ETRAN.[3] The cumulative probability distribution is expanded in Legendre polynomials:

$$G_N(\theta) = H_{max} + \sum_{o}^{\ell_{max}} (\ell + \tfrac{1}{2})(H_\ell - H_{max}) \int_o^\theta P_\ell(\cos\theta')\,\sin\theta'\,d\theta' \tag{76}$$

where

$$H_\ell = \exp\left\{-\int_s^{s+s_N} S_\ell(s')ds'\right\} \tag{77}$$

and

$$S_\ell(s) = 2\pi N \int_{-1}^{1} \sigma(\theta,s)\ [1 - P_\ell(\cos\theta)]d(\cos\theta) \tag{78}$$

σ is the Mott single scattering cross section with the screening correction of Moliere. The coefficients S_ℓ are calculated using the procedures of the SING subroutine of ETRAN. The coefficients H_ℓ are calculated using the procedures of the MULT subroutine of ETRAN. The term H_{max} represents the probability of zero scatter over the pathlength increment,

$$H_{max} = \lim_{\ell\to\infty} H_\ell \ . \tag{79}$$

Separation of this term from the Legendre expansion considerably improves the series convergence at low energy, as discussed in Reference 12. The integrals of the Legendre polynomials,

$$Q_\ell = \int_0^{\theta} P_\ell\ (\cos\theta')\ \sin\theta'\ d\theta' \tag{80}$$

are evaluated through recursion.

Section 5

USER INFORMATION

POEM is a FORTRAN computer program coded for the CDC 6400, 6600, or 7600 computer. (A version coded for the IBM 370/195 computer is also available.) The code is obtainable on seven track, 556 bpi tapes. Two tapes are required for operation: one contains the photon interaction data file; the other contains the program source decks in the CDC UPDATE format. Five codes are contained on the program tape, identified by UPDATE DECKNAMES: EDITOR, DATAGEN, 1S1D, 1S2D, and 2S. EDITOR reads the photon interaction data tape and writes a selected subset of data on disk or tape. DATAGEN creates an electron interaction data file on disk or tape. 1S1D and 1S2D are the one- and two-dimensional x-ray photoemission transport programs. 2S is the x-ray transition zone dose transport program.

A transport calculation requires a photon interaction data file (lfn* = TAPE8), an electron interaction data file (lfn = TAPE16) and a card input which defines the transport media, the photon spectrum, and electron source parameters. The procedures for creating the data files and running the transport programs are outlined in the succeeding paragraphs.

---

* local file name

5.1 PHOTON INTERACTION DATA FILE CREATION

The EDITOR code permits the creation of a truncated photon data set on permanent disk file from a subset of the photon data set on the tape file. This subset can be larger than the set required for a given transport calculation; the transport program searches the file for the data required for a particular run. The recommended procedure is to create a permanent disk file with as many elements as anticipated to be required for a series of calculations.

A run requires the EDITOR program, the photon interaction data tape (lfn = TAPE1), and a card input. The program creates a photon interaction data file (lfn = TAPE2) to be cataloged on permanent disk file.

The card input consists of two to four cards:

CARD	FORMAT	DESCRIPTION
1	I5	Number of elements to be put in file (max 25)
2-4	10I5	List of element atomic numbers in ascending order

It is essential that the element atomic numbers be listed in ascending order so that the transport program can properly search through the file.

The printer output confirms the copying of the interaction data for each element.

5.2 ELECTRON INTERACTION DATA FILE CREATION

The DATAGEN code creates the electron interaction data file on disk or tape. A run requires the DATAGEN program and a card input. The program creates a data file (lfn = TAPE16). Once an electron data set for a material

has been created on permanent disk file or tape, that set can be used for any transport calculation in that material, for any electrons of energy equal to or less than the maximum electron energy in the file (EEMAX).

5.2.1 Input

The card input is in the NAMELIST format. This format is convenient for the input of optional parameters. One or two NAMELISTS are used: POET and ELIST1. ELIST1 is required only if it is desired to vary the logarithmic spacing of the transport energy grid as discussed in Section 3.2.3. (POET is always required to create a POEM.) The NAMELIST input variables are defined below.

NAMELIST/POET/

For a material composed of a single element the variables defining the material are

Z(1)* = atomic number
A(1) = atomic weight

For a material composed of several elements, the variables defining the material are:

LMENT = number of elements (max 8)
Z(1) = list of atomic numbers
A(1) = list of atomic weights
W(1) = list of weight fractions

---

* Notation: For the NAMELIST input of an array, the CDC computer demands the index of the first element, for example Z(1) = 1, 6, 7, 8. We denote herein all arrays by the format VAR(1) = ...

The variables defining the transport energy grid are:

EEMAX = maximum electron energy in MeV, ($\leq$10 MeV)

(If one is creating an electron data set on permanent disk file or tape, then one should set EEMAX = 10 so that the file will be valid for any POEM calculation for that material, unless of course one does not anticipate any calculation for electron energies greater than some limit EEMAX<10 MeV.)

NSUB = number of substeps per logarithmic step [Equation (45)]

If one does not want to vary the logarithmic spacing of the transport energy grid between the maximum energy (EEMAX) and the minimum energy (0.001 MeV), then one inputs

NCYC = the number of logarithmic steps to reduce the electron energy by a factor of one-half [Equation (44)]. The recommended value is 8.

If one does want to vary the logarithmic spacing of the transport energy grid, as discussed in Section 3.2.3, then one does not input NCYC but inputs the NAMELIST ELIST1 as described below.

NAMELIST/ELIST1/

ELIST1 is input only if one wants to vary the logarithmic spacing of the transport energy grid. The variables are

NCMAX = number of energy grid points at which the logarithmic spacing is to change (max 10)

TC(1) = list of energies (MeV) at which the spacing is to shift

(Unless one wants to terminate the electron trajectories at some minimum energy greater than 0.001 MeV, set TC(NCMAX) = 0.001.)

NCYC1(1) = list of NCYC values [Equation (44)]

(NCYC1(1) determines the logarithmic spacing between EEMAX and TC(1); NCYC1(2) determines the logarithmic spacing between TC(1) and TC(2); ...; NCYC1(NCMAX) determines the logarithmic spacing between TC(NMAX-1) and TC(NMAX). See Section 3.2.3 for discussion of the spacing.)

NDMAX = number of energy grid points at which the multiple scattering distribution is to be printed (max 10)

ND(1) = list of energy grid point index numbers at which the multiple scattering distribution to be printed (e.g., if ND(1) = 1, 10, 25, then the distributions are printed at E, E_{10}, and E_{25}

(It is recommended that the multiple scattering distribution be printed at least at every grid point at which the logarithmic spacing changes. If one uses the option of inputting NCYC in the POET NAMELIST, then the ND values are internally set to ND(1) = 1, NCYC+1, 2NCYC+1, ...)

5.2.2 Output

The NAMELIST inputs are printed out, complete with the default values for the variables not input.

The multiple scattering distribution is printed at each of the grid points ND(1), ND(2), ..., NDMAX. This output includes:

N = energy grid point

E = energy within the energy bin for which the printed distribution is calculated

S = residual range (g/cm^2)

DELTAS = pathlength increment (g/cm^2 and in mean-free-pathlengths)

MFP = transport mean-free-pathlength (g/cm^2)

MEAN(COS) = mean cosine of angle through which electron is deflected

PROB(NO SCATTER) = probability of zero scatter along pathlength increment

SINGLE SCATTERING LEGENDRE COEFFICIENTS
= $r_o S_\ell$, $\ell=1, \ell_{max}$, where r_o=residual range and the coefficients S_ℓ are given by [Equation (78)]

MULTIPLE SCATTERING LEGENDRE COEFFICIENTS
= $H_\ell - H_{max}$, $\ell=1, \ell_{max}$, where the coefficients H_ℓ are given by [Equation (77)]

(The multiple scattering coefficients must monotonically converge to zero.)

CUMULATIVE MULTIPLE SCATTERING DISTRIBUTION
= $G_N(0)$, $0=0, \pi$, [Equation (76)]

(The distribution must converge monotonically to one.)

The end point deflection angles for the multiple scattering distribution are printed.

The electron slowing down spectrum is printed. This output includes: N = index number of logarithmic grid, energy, stopping power - collision, radiation, and total - step size (pathlength increment), and mean penetration in the electron initial direction.

5.3 X-RAY PHOTOEMISSION CALCULATION

The Monte Carlo codes, deck names 1S1D and 1S2D, calculate the x-ray photoemission from a planar surface. For cases of normal photon incidence or when the two-dimensional description of the emission angular distribution is not required the 1D version should be used since it is a significantly faster code. A run requires the transport program, a photon interaction data file (lfn = TAPE8) containing the elements of the material, the electron interaction data file (lfn = TAPE16) for the material, and a card input.

5.3.1 Input

The card input consists of three NAMELISTS - MEDIA defining the material, PHOTON defining the photon spectrum, and ESOURC defining source parameters - and a time limit card. The deck structure is

MEDIA
PHOTON
ESOURC
time limit (CP seconds in F10.0 format)

The variables of the NAMELISTS are defined in the succeeding paragraphs.

NAMELIST/MEDIA/

MEDIA defines the electron emitting material. For a material composed of a single element the composition is defined by a single variable

NZEL(1) = atomic number

For a composition of several elements the variables are

NELMTS = number of elements (max 10)
NZEL(1) = list of atomic numbers
PCOMP(1) = list of weight fractions

For a thick slab ($\Delta z \geq R_e$) the emission is independent of thickness; no input requiring thickness or density is required. For a thin foil ($\Delta z < R_e$) the thickness may be input in one of three ways:

(a) TKCMS = thickness in g/cm^2
(b) TKCMS = thickness in cm
RHO = density (g/cm^3)
(c) TKINS = thickness in inches
RHO = density (g/cm^3)

NAMELIST/PHOTON/

PHOTON defines the photon energy spectrum and angle of incidence. Three options are available for defining the spectrum:

(a) monochromatic spectrum
TBL(1) = photon energy (keV)
(b) arbitrary spectrum
NHNU = number of photon energy groups (max 120)
TBL(1) = list of mid-points of the energy bins (keV)
WIDTH(1) = list of widths of the energy bins (keV)
EII(1) = list of the fractions of the photon energy fluence in each energy bin
(c) black body spectrum
T = spectrum temperature (keV)

The default angle of incidence is zero (normal incidence). For oblique incidence input

ANG = angle of incidence with respect to surface normal (degrees)

For back emission one can either input ANG>90°, or input ANG<90° and set NSIGN = -1 in the ESOURC NAMELIST.

NAMELIST/ESOURC/

ESOURC sets parameters defining the electron source. The only required input is

IMAX = number of particle histories to be run (the default value is 1000)

Normally the program prints the marginal source distributions S'(E) and S'(θ) but not the joint distribution S'(E,θ). To suppress the print of the marginal distributions set

MARGIN = 0

To print the joint distribution set

JOINT = 1

One can specify back emission by setting the photon angle of incidence ANG with respect to the surface outward normal greater than 90°. Alternatively one can use the angle with respect to the inward surface normal (<90°) and set

NSIGN = -1

For the 2D code the number of azimuthal (ϕ) output angle bins is 8 by default. To change the number of ϕ bins set

NPHI = number of ϕ angle bins (max 10)

The maximum electron energy in the source distribution is by default equal to the maximum photon energy, TBL(NHNU). To reduce this maximum energy set

EEMAX = maximum electron energy (keV)

The number of electron energy groups and the number of electron angle groups in the source distribution are by default equal to 20, the maximum. To reduce the number of source groups (correspondingly reducing the number of groups in the output distribution) set

NEE = number of energy groups
NTH = number of angle groups

5.3.2 Output

The program prints out the NAMELIST inputs, complete with the default values of the variables not inputted. The photon spectrum representation is printed. Confirmation is printed of the elements read from the photon interaction data file.

The source material definition is printed: composition, thickness, and density. The electron source density S(electrons/cm^2) and the electron source density distribution with respect to photon energy S'(hν)(electrons/cm^2) are printed. For MARGIN = 1 (default value = 1) the one-dimensional, marginal, electron source energy and angular distributions S'(E) and S'(θ) are printed. For JOINT = 1 (default value = 0) the two-dimensional, joint distribution S'(E,θ) is printed.

The program prints the case - fore or back emission - the photon angle of incidence, and the mean photon energy. Transport diagnostic parameters are printed: the number of particle histories run (if the run time-limits, this

will be less than IMAX), the number of particle emissions, the fractional number of emissions per history, the mean probability of electron emission from the source region (since the particles have various weights, this probability differs from the fractional number of emissions per history), the mean number of trajectory steps per particle emission, and the mean angular deflection of the emitted electrons (with respect to their original direction).

The electron yield is calculated in units of electrons/photon, coul/cal, and cal(electron)/cal(photon).

The following moments of the distribution of the electron yield are calculated:

$\langle E \rangle$ = mean energy

$\langle \cos\theta \rangle = \langle \vec{\Omega} \cdot \hat{z} \rangle$ = mean direction cosine with respect to $\hat{z}$ (the surface outward normal)

$\langle \cos 2\theta \rangle$

$\langle \sin\theta\cos\phi \rangle = \langle \vec{\Omega} \cdot \hat{x} \rangle$ = mean direction cosine with respect to $\hat{x}$ (the projection of the photon direction vector on the material surface)

$\langle \cos\phi \rangle$

J_z = yield (electrons/photon) = the z-component of the emission current (normal to the surface)

J_x = the x-component of the emission current (parallel to the surface)

J_x/J_z

The one-dimensional distributions of the electron yield are printed:

y'(E) = energy spectrum

y'(θ) = polar angular distribution (with respect to surface normal)

$y'(\phi)$ = azimuthal angular distribution (with respect to the plane of the photon direction vector and the surface normal)(for oblique incidence only; for normal incidence $y'(\phi)$ is uniform over $(0,2\pi)$

[In future versions of the code it is planned to add the one-dimensional distributions

$y'(\cos\vartheta)$

$y'(\sin\theta\cos\phi)$]

The two- and three-dimensional distributions of the electron yield are written on disc for economy of printed output (lfn = TAPE13). The file may be saved for later analysis by cataloging as a permanent disk file or tape or printed by rewinding TAPE13 and copying it into OUTPUT. The distributions are

$y'(\theta,\phi)$

$y'(E,\theta)$

$y'(E,\phi)$

$y'(E,\theta,\phi)$

5.4 X-RAY TRANSITION ZONE DOSE CALCULATION

Calculation of the transition zone dose and current near a planar interface requires the transport program - deck name 2S - a photon interaction data file (lfn = TAPE8) containing the elements in the electron source material, an electron interaction data file for the two interfacing materials, and card input. The electron data file can be created in one of two ways: (1) set MEDMX = 2 in the POET NAMELIST input for DATAGEN for the data calculation for material A, and input a second complete card input (without specifying MEDMX) for material B in the same run; or (2)

independently create two data files - one for material A, one for material B - and then create a single file through the procedure:

```
COPYBF(A,TAPE16)
BKSP(TAPE16)
COPYBF(B,TAPE16)
REWIND(TAPE16)
```

5.4.1 Input

The same three NAMELIST inputs and time limit card are required as in the x-ray photoemission calculation - the deck structure is the same. The PHOTON and the ESOURC NAMELIST inputs are the same. The only differences are in the NAMELIST MEDIA. Refer to Section 3.3 for the definition of the problem geometry and discussion of the computational procedures.

NAMELIST/MEDIA/

The identification of the electron source material is controlled by MSOURC. For MSOURC = 1 (the default value) the source is in material A; the program calculates dose and current distribution in material B due to electron emission from material A. For MSOURC = 2 the source is in material B; the program calculates the dose and current in material B due to electron backscatter from material A.

The variables defining the electron source material composition are the same as for the x-ray photoemission calculation. One only inputs the composition definition variables (NELMTS, NZEL, PCOMP) for the source material - if MSOURC = 1, material A; if MSOURC = 2, material B.

If the materials are each thicker than the maximum electron range, then the dose and current profiles are

independent of thickness. The thicknesses are by default set equal to the maximum electron ranges - no input is required. For foils thinner than the electron range, the thicknesses may be defined in one of three ways:

(a) TKCMS(1) = thickness (A), thickness (B) (g/cm^2)

(b) TKCMS(1) = thickness (A), thickness (B) (cm)

DENS(1) = density (A), density (B)(g/cm^3)

(c) TKINS(1) = thickness (A), thickness (B) (inches)

DENS(1) = density (A), density (B)(g/cm^3)

5.4.2 Output

The first part of the program output - NAMELIST inputs, photon spectrum representation, elements read from photon data file, source material definition, and electron source density and distributions - are identical to the x-ray photoemission output. A diagnostic indicating the number of materials for which electron interaction files were read is printed.

For MSOURC = 1 the transport diagnostic parameters printed are: the number of particle histories; the number of particles emitted from material A into material B; the number of particles backscattered from B; the electron yield from A in electrons/photon, coul/cal, and cal(electron)/cal(photon); and the charge and energy backscatter yields from B (dimensionless). For MSOURC = 2 the transport diagnostic parameters printed are: the number of particle histories; the number of particles emitted from B into A; the number of particles backscattered from A, the electron yield from B in electrons/photon, coul/cal, and cal(electron)/cal(photon); and the charge and energy backscatter yields from A (dimensionless).

For MSOURC = 1 the energy and angular distributions of the electron yield from A, $y'(E)$ and $y'(\theta)$, are printed. For MSOURC = 2 the energy and angular distributions of the electron backscatter yield from A are printed.

The electron current (electrons/photon) and energy current (cal(electron)/cal(photon)) are printed at each deposition zone boundary. For MSOURC = 1 this is the current emitted from material A; for MSOURC = 2 it is the current backscattered from A. These currents are finite differenced to obtain the charge deposition, (electrons/g)/(photon/cm^2), and energy deposition, (cal/g)/(cal/cm^2) = cm^2/g, in each deposition zone.

The electron charge and energy currents are fit by expressions of the form

$$y = A \exp(Bz + Cz^2 + Dz^3)$$

The fit coefficients A, B, C, and D, the fit representations of the currents at each deposition zone boundary, and the percentage difference between the fit and Monte Carlo representations of the currents at each zone boundary are printed. The fit expression is analytically differentiated to obtain the fit representations of the energy and charge depositions. The fit representations of the depositions and the percentage difference with respect to the Monte Carlo finite difference representations are printed for each deposition zone.

REFERENCES

1. W.L. Chadsey and C.R. Ragona, "Proceedings of National Symposium on Radiation in Space," NASA TM-X2440, 786 (1972).

2. H.M. Colbert, "SANDYL," Sandia Laboratories, SLL-74-0012 (1974).

3. M.J. Berger and S.M. Seltzer, Electron and Photon Transport Programs, (I) NBS Report 9836, (II) NBS Report 9837.

4. T. Jordan, "BETA-II," A.R.T. Research Corporation, ART-60 (1971).

5. T.A. Dellin and C.J. MacCallum, IEEE Trans. Nuc. Sci., NS-20, No. 6, 91 (1973).

6. O. Lopez, "A Simple Analytical Calculation of X-Ray Photoemission," DNA Symposium on TREE/SGEMP/IEMP (1975).

7. J.C. Garth and J.V. O'Brien, IEEE Trans. Nuc. Sci., NS-20, No. 6, 82 (1973).

8. E. Wenass and M. Williams, Unpublished.

9. O. Lopez and W.F. Rich, IEEE Trans. Nuc. Sci., NS-20, No. 6, 14 (1973).

10. W.L. Chadsey and I. Kohlberg, IEEE Trans. Nuc. Sci., NS-18, No. 6, 150 (1971).

11. W.L. Chadsey and C. Woodrow Wilson, "X-Ray Photoemission: Analytical, Monte Carlo, and Multidimensional Calculations," Submitted to 1975 IEEE Conf. on Radiation Effects.

12. J.C. Garth and W.L. Chadsey, Unpublished.

REFERENCES (Continued)

13. J.N. Bradford, IEEE Trans. Nuc. Sci., NS-20, No. 6, 105 (1973).

14. W.L. Chadsey, "Transition Zone Dose in Multilayer Device," SAI EMP/SV Technical Note 75-WA-3 (April 1975).

15. W.L. Chadsey, "Monte Carlo Calculations of Dose Distribution in SEM Irradiated Semiconductor Structures," NAD Crane TR/7024/C74/64 (1973).

16. W.L. Chadsey, IEEE Trans. Nuc. Sci., NS-21, No. 6, 235 (1974).

17. J.M. Hammersley and D.C. Handscomb, Monte Carlo Methods, Methuen & Co., Ltd., London (1964).

18. E.J. McGrath and D.C. Irving, "Techniques for Efficient Monte Carlo Simulation," SAI-72-590-LJ (1972).

19. E. Storm and H.I. Israel, Photon Cross Sections from .001 to 100 MeV for Elements 1 through 100, LA-3753, LASL (1967).

20. T.A. Dellin and C.J. MacCallum, "A Handbook of Photo-Compton Current Data," Sandia Laboratories SCL-RR-720086 (1972).

21. R.D. Evans, The Atomic Nucleus, McGraw-Hill, New York (1955).

22. C.M. Davisson and R.D. Evans, Rev. Mod. Phys., 24, 79, (1952).

23. D.J. Dudziak, "ENDF Formats and Procedures for Photon Production and Interaction Data," LA 4549, LASL (1971).

24. C.J. MacCallum and T.A. Dellin, J. Appl. Phys., (April 1973).

25. W. Bambynek, et al., Rev. Mod. Phys., 44, 716 (1972).

REFERENCES (Continued)

26. M.J. Berger and S.M. Seltzer, "Tables of Energy Losses and Ranges of Electrons and Positrons," NASA SP-3012.

27. H.W. Koch and J.W. Motz, Rev. Mod. Phys., 31, 920 (1959).

28. W.L. Chadsey and V.W. Pine, "POEM Code Calculations of X-Ray Photoemission using an Orthonormal Polynomial Expansion Technique," EMP/SV Technical Note 75-WA-1, SAI (1975).

29. W.L. Chadsey, E.R. Parkinson, and V.W. Pine, "Source Region EMP Calculations," SAI-75-502-WA, SAI (1975).

30. R.D. Evans in F.H. Attix and W.C. Roesch, Radiation Dosimetry, Vol I, 105, Academic Press, New York (1968).

31. R.H. Fisher and J.W. Wiehe, "A User's Guide to the FSCATT Code," Systems, Science, and Software, 3SR-318 (1970).

32. E.A. Straker, W.H. Scott, and N.R. Byrn, "The MORSE Code with Combinatorial Geometry," DNA 2860T (1972).

DISTRIBUTION LIST

DEPARTMENT OF DEFENSE

Director
Armed Forces Radiobiology Research Institute
Defense Nuclear Agency
ATTN: Robert E. Carter

Defense Documentation Center
Cameron Station
ATTN: TC (12 copies)

Director
Defense Nuclear Agency
ATTN: RAEV, LTC J.M. Daley
ATTN: STTL, Technical Library (3 copies)
ATTN: DDST
ATTN: DDST, Peter H. Haas
ATTN: RATN
ATTN: SPVL
ATTN: SPSI

DEPARTMENT OF THE ARMY

Director
Ballistic Missile Defense Advanced
Technical Center
Huntsville Office
ATTN: BDMH-O, F.M. Hoke

Commander
Harry Diamond Laboratories
ATTN: AMXDO-RBG, Robert E. McCoskey
ATTN: AMXDO-RB, Edward E. Conrad
ATTN: AMXDO-RBF, John E. Tompkins
ATTN: AMXDO-PBI, John A. Rosado
ATTN: AMXDO-RC, Robert B. Oswald, Jr.
ATTN: AMXDO-RBH, Paul A. Caldell
ATTN: George Merkel

Director
U.S. Army Ballistic Research Laboratories
ATTN: AMXBR-RL, Mr. Harrison
ATTN: AMXRD-BRD, Dr. Eccleshall

Commander
U.S. Army Electronics Command
ATTN: AMSEL-NL-D
ATTN: AMSEL-TN-N, Dr. E. Both
ATTN: AMSEL-WL-D

Commander
U.S. Army Nuclear Agency
ATTN: ATCN-W, LTC Leonard A. Sluga

DEPARTMENT OF THE NAVY

Chief of Naval Research
Department of the Navy
ATTN: Code 422

Commander
Naval Electronics Laboratory Center
ATTN: Code 3200, H.F. Wong
ATTN: Code 3100, E.E. McCown

DEPARTMENT OF THE NAVY

Superintendent
Naval Postgraduate School
ATTN: Code 2124, Tech Rpts Librarian

Director
Naval Research Laboratory
ATTN: Code 5210, John E. Davey
ATTN: Code 4004, Emanual L. Brancato
ATTN: Code 5216, Harold L. Hughes
ATTN: Code 6460, Dean L. Mitchell
ATTN: Code 6631, James C. Ritter
ATTN: Code 6603F, Richard L. Statler

Commander
Naval Surface Weapons Center
ATTN: Code 730, Technical Library (6 copies)
ATTN: Code 431, John H. Malloy

Director
Strategic Systems Project Office
Navy Department
ATTN: NSP-2342, Richard L. Coleman
ATTN: NSP-230, David Gold
ATTN: NSP-27331, Phil Spector

DEPARTMENT OF THE AIR FORCE

Air Force Cambridge Research Laboratories
AFSC
ATTN: LQD, Russell P. Dolan, Jr.
ATTN: LQD-STOP 30, Freeman Shepherd
ATTN: LQR, Edward A. Burke (20 copies)
ATTN: SURRP (13 copies)
ATTN: SURRA (5 copies)
ATTN: SUOLA S29 (2 copies)
ATTN: XOP
ATTN: LQR, C.A. McCartney (10 copies)

Air Force Institute of Technology, AU
ATTN: ENP, Charles J. Bridgeman

Air Force Weapons Laboratory, AFSC
ATTN: ELP, TREE Section
ATTN: SAA
ATTN: SAY

SAMSO/DY
ATTN: DYS, Major Larry A. Darda
ATTN: DYS, Major Heilman
ATTN: DYS, Captain W. Mercer

SAMSO/MN
ATTN: MNNH, Captain William M. Carra
ATTN: MNNH, Captain Salch

SAMSO/RS
ATTN: RSSE, LTC Kenneth L. Gilbert
ATTN: RSE

SAMSO/XR
ATTN: XRS

UNITED STATES ENERGY RESEARCH AND DEVELOPMENT ADMINISTRATION

Los Alamos Scientific Laboratory
ATTN: Doc Con for Donald R. Westervelt

Sandia Laboratories
Livermore Laboratory
ATTN: Doc Con for Kenneth A. Mitchell, 8157
ATTN: Doc Con for J.A. Mogford, 8341
ATTN: Doc Con for Theodore A. Dellin
ATTN: Doc Con for Kenneth W. Dolan

Sandia Laboratories
ATTN: Doc Con for J.V. Walker, 5220
ATTN: Doc Con for E.F. Hartman
ATTN: Doc Con for F.N. Coppage, 1933
ATTN: Doc Con for J.A. Hood, 2110
ATTN: Doc Con for C.N. Vittitoe, 5223
ATTN: Doc Con for J.E. Gover, 1935
ATTN: Doc Con for C.J. MacCallum

University of California
Lawrence Livermore Laboratory
ATTN: Walter W. Hofer, L-153
ATTN: William J. Hogan, L-531
ATTN: Leroy M. Erickson, L-24
ATTN: Hans Kruger, L-94

OTHER GOVERNMENT

Department of Commerce
National Bureau of Standards
ATTN: Appl Rad Div, Robert C. Placious
ATTN: Judson C. French

NASA
ATTN: Code Res Guid Con & Info Sys

NASA
Lewis Research Center
ATTN: Library

DEPARTMENT OF DEFENSE CONTRACTORS

Aeronutronic Ford Corporation
Western Development Laboratories Division
ATTN: Donald R. McMorrow, MS G30

Aerospace Corporation
ATTN: R. Mortensen
ATTN: L.W. Aukerman
ATTN: William W. Willis
ATTN: Library
ATTN: Melvin J. Bernstein
ATTN: J. Benveniste

Battelle Memorial Institute
ATTN: STOIAC

Bell Telephone Laboratories, Inc.
ATTN: R.D. Taft, 2B-181
ATTN: H.A. Jarrell, WH-2F-153

DEPARTMENT OF DEFENSE CONTRACTORS

Boeing Company, The
ATTN: A.R. Lawrey, MS 2R-00

Communications Satellite Corporation
ATTN: Richard A. Arndt

General Electric Company
Space Division
ATTN: Daniel Edelman

General Electric Company
Re-Entry & Environmental Systems Division
ATTN: John W. Palchefsky, Jr.
ATTN: Robert V. Benedict

General Electric Company
Tempo-Center for Advanced Studies
ATTN: DASIAC (20 copies)

Honeywell Incorporated
Aerospace Division
ATTN: Harrison H. Noble, MS 725-5A

Hughes Aircraft Company
ATTN: John B. Singletary, MS 6-D133

INTELCOM Rad Tech
ATTN: Ralph H. Stahl
ATTN: MDC
ATTN: Technical Library
ATTN: James A. Naber
ATTN: Eric P. Wenaas

Johns Hopkins University
Applied Physics Laboratory
ATTN: Peter E. Partridge

Kaman Sciences Corporation
ATTN: W. Foster Rich
ATTN: Frank H. Shelton

Lockheed Missiles and Space Company
ATTN: Clarence F. Kooi, 52-11

Maxwell Laboratories, Inc.
ATTN: V. Fargo

MITRE Corporation, The
ATTN: M.E. Fitzgerald

Mission Research Corporation
ATTN: Technical Library

Northrop Corporation
Northrop Research and Technology Center
ATTN: David N. Pocock
ATTN: James P. Raymond
ATTN: Library

Physics International Company
ATTN: Doc Con for John H. Huntington
ATTN: Doc Con for Charles H. Stallings
ATTN: Doc Con for Philip W. Spence
ATTN: Doc Con for Technical Library

DEPARTMENT OF DEFENSE CONTRACTORS (Continued)

Pulsar Associates, Inc.
ATTN: Carleton H. Jones, Jr.

R & D Associates
ATTN: Richard R. Schaefer
ATTN: Robert A. Poll
ATTN: S. Clay Rogers

Science Applications, Inc.
ATTN: William L. Chadsey (20 copies)

Science Applications, Inc.
ATTN: Charles Stevens

Simulation Physics, Inc.
ATTN: Roger G. Little

Stanford Research Institute
ATTN: Robert A. Armistead

Systems, Science and Software
ATTN: Alan F. Klein

Systems, Science and Software
ATTN. Andrew R. Wilson
ATTN: Technical Library

Texas Instruments, Inc.
ATTN: Sanders B. Cox, Jr., MS 909

TRW Systems Group
ATTN: A. Anderman, R1-2036
ATTN: R.D. Loveland, R1-2036
ATTN: Lillian G. Singletary, R1-1070
ATTN: Paul Molmud

Van Lint, Victor A.J. (Consultant)
ATTN: V.A.J. Van Lint

Westinghouse Electric Corporation
Research & Development Center
ATTN: William E. Newell